SLOCUM GLIDER:
Design and 1991 Field Trials

Prepared by:
Paul Simonetti
Webb Research Corp.
under subcontract from

Woods Hole Oceanographic Institution
Office of Naval Technology
Contract No. N00014-90C-0098

September 1992

ABSTRACT

A prototype SLOCUM glider was fabricated and tested in open-loop, shallow water field trials in January 1991. Straight-ahead and turning dives were accomplished using a fixed-weight release to produce the buoyancy changes that drive the sinking and ascent modes. Average horizontal glide speeds of .13 m/sec and turn radii of 21-70 m were obtained, in good agreement with computer simulated predictions. A separate pool test showed that gliding at very shallow (5°-7°) angles with the horizontal could be initiated, although such a mode is inherently unstable.

An advanced, autopilot-controlled glider was designed and successfully tested at Seneca Lake, NY in November 1991. It employed a hydraulic pump to inflate an external bladder as the means of changing buoyancy for ascent/descent. Average horizontal glide speed of .20 m/sec and turn radii of 7-13 m as well as course-correction performance in excess of expected future ocean deployment needs were obtained.

Specifications for a 5-year endurance, .28 m/sec horizontal speed ocean glider, with an ocean thermocline-driven buoyancy change engine are presented.

TABLE OF CONTENTS

LIST OF FIGURES

I. INTRODUCTION

This report presents the design features, computer-simulated and actual field trial gliding and autopilot performance of the first two models in the ongoing evolution of the SLOCUM glider vehicle. The vehicle mission is to gather oceanographic data while performing autonomous, gliding dives to 1800 m depth at typical glide path angles of 45° with the horizontal, and a sink rate of .33 m/sec (Figure 1). The ascent/descent portions of the dives are driven by the vehicle's ability to slightly (typ ±100 g) change its net buoyancy at the inflection points of the dive. The energy to power these buoyancy changes will eventually be provided at zero on-board energy cost by a heat engine that exploits the ocean's thermal gradient between the warm surface and cold deep layers of the ocean. The first two units described in this report employed mechanical, energy consuming means of buoyancy change.

The glider is a faired cylinder with fixed vertical and horizontal wings at the aft end. These provide gliding lift as well as stability and steering moments. The cylindrical fuselage also provides some lift. The vehicle pitch angle is changed by longitudinal movement of an internal weight. The vehicle roll angle is changed by rotation about the vehicle centerline of the same radially asymmetric, internal, moveable weight. This causes the fixed wings to rotate and produce a net lateral yawing moment due to their vertical/horizontal asymmetry; as a result, the vehicle changes its heading. Once per day, the vehicle will assume a vertical, antenna-up position at the surface and eventually engage in two-way satellite communication. This maneuver is accomplished by activating approximately 0.7 liter of additional surface buoyancy in the vehicle nose and by movement of the vehicle's center of gravity aft-ward and on-centerline. Power to activate the surface buoyancy will be provided at no on-board energy cost by a second heat engine. This engine will operate on a different thermodynamic cycle than the drive buoyancy engine. The long-term deployment target is 5 years.

A basic description of the design features and field trial environment of the first two glider models follows.

1. Prototype Glider (Figure 2)

Physical Description

Mass : 39.8 kg
Length : 1.9 m (fuselage); 2.8 m (overall including antenna, wings)

Pressure Hull
Diameter :0.165 m
Material :6061-T6 aluminum
Collapse Depth : 2600 m
Length: 1.52 m

Wings
Configuration: Rectangular Box-Tail
Area : 0.023 m^2 (Vertical) 1.0 aspect ratio (AR)
(each) 0.047 m^2 (Horizontal, small size) 2.0 AR
0.071 m^2 (Horizontal, medium size) 3.0 AR
0.094 m^2 (Horizontal, large size) 4.0 AR
Material: Fiberglass covered syntactic foam
Thickness:10.2 mm (max.)

Vehicle Characteristics

Buoyancy Change: ±39 g net about neutral; pressure commanded, electromagnet-released drop weight on vehicle nose.
Radial CG offset from centerline: 2.4 mm
Sink rate @ 40°
Pitch angle: 0.10 m/sec (medium wings)
Vehicle controller and Data Logger: Onset Computer Corp.; Tattletale Model II
Dive Variables Stored:
- vehicle heading
- vehicle pitch angle
- vehicle roll angle
- pitch actuator position
- roll actuator position
- battery voltage
- ambient pressure
- time

Heading sensor: Watson Industries, custom 3 axis fluxgate compass with pitch and roll outputs.
Pressure sensor: Transmetrics Model P21LC (0-50 psig)
Depth Telemetry/Emergency Release Sonar: Benthos Model 865, 10 kHz (x-mit), 12 kHz (receive)
Antenna: 0.66 m long x 10.2 mm dia whip (non-functional)
Battery capacity: 18 alkaline D cells, 2 parallel banks @ 13.5V/bank
Current drain: 5 ma (quiescent); 500 ma (peak)

Field Trial Description

A series of twenty nine (29) dives was run at Wakulla Springs, Florida, in January 1991 with the prototype glider. The tests exercised the gliding and turning dynamics of the vehicle for the three different sized steering wings over the range of vehicle roll angles. The specific geometry of the test site (Figure 3) required the dives be run near glide angles of 40° with the horizontal and that turn-around depths be less than 60 feet. The site was chosen for its exceptional

water clarity and its reasonable depth in an unobstructed, relatively confined area. This allowed direct observation of the vehicle at all times through a glass-bottom boat to visually verifiy gliding, as well to track and to retrieve it easily.

The typical deployment sequence began with programming the glider with dive parameters at the surface through a serial communicator port. The communicator would then be disconnected, the nose drop-weight attached, the vehicle pointed in the proper direction and let go in an approximately horizontal attitude. The unit would quickly pitch down to its proper dive angle, dive to its weight-drop depth, drop the weight and then pitch up for its ascent glide and subsequent re-surfacing. The glass-bottom boat would then come alongside the surfaced vehicle for reattachment of the communicator cable. Dive data would be offloaded and new parameters downloaded for the next dive while the vehicle was towed back to the original launch point. The entire launch, retrieval and reprogramming sequence could be done in 20 minutes.

Following the Wakulla Spring tests, a brief test was conducted at the 20 X 20 X 20 ft. pool at Benthos Inc., North Falmouth, MA, to determine the minimum angle at which the vehicle would continue to glide and not stall. This was done by pushing the vehicle to the bottom of the pool in the buoyant, ascent condition (without the nose weight). The ascent pitch angle with the horizontal was decreased until the vehicle was observed to ascend straight up (stalled) and no longer glide.

2. Lake Test Glider (Figure 4)

Physical Description

(Same as prototype unit except as follows.)

Mass: 40.3 kg
Length: 2.0 m (fuselage); 3.2 m (overall including antenna, wings)

Wings

Configuration: Straight cruciform, swept platform
Area: 0.036 m^2 (Vertical), 66° sweepback, 3.9 AR
(each) 0.067 m^2 (Horizontal), 43° sweepback, 1.6 AR
Thickness: 15.9 mm (max.)

Vehicle Characteristics

Buoyancy Change: ±50 g net about neutral; pressure commanded hydraulic pump driven oil inflation of external bladder in tail cone fairing
Radial CG offset from centerline: 3.8 mm

Sink rate @ 40° pitch angle: 0.17 m/sec
Pressure sensor: Transmetrics Model P21LC (0-500 psig)
Autopilot: See Figure 5 for block diagram

Field Trial Description

A series of 15 ascent glides were performed at a test pool at Raytheon Co., Submarine Signal Division, Portsmouth, RI, on November 5, 1991. The section of the pool used for the tests was 20 ft. wide X 20 ft. deep X 40 ft. long. The glider was pushed to the bottom in the buoyant condition (external oil bladder inflated) at one end of the pool with a collared pole. It was positioned to point down the 40 ft. length of the pool and disengaged from the pole. The vehicle would pitch up to its intended angle and glide down the pool while ascending. Its open-loop gliding and turning characteristics were exercised over several pitch angles and the full range of vehicle roll angles, right and left.

A series of 14 autopilot trial dives were performed out of Watkins Glen, NY, on Seneca Lake during November 10-14, 1991. The vehicle was deployed from a 29 ft., large cockpit cruiser in the general location shown on the chart in Figure 6. The vehicle was programmed for the current dive on deck, deployed, retrieved and brought back onboard for data downloading and programming for the next dive.

The tests' purpose was to determine the ability of the autopilot to come to and hold a programmed heading over a range of initial off-course errors (right and left) for various values of autopilot gain. A typical dive would have the vehicle released from the surface at some initial deviation from its programmed heading, with the steering wings level and the pitch approximately horizontal. The vehicle would pitch and glide down while the autopilot rolled the vehicle appropriately to correct the heading error, and then hold the desired course until reaching the depth that activates the buoyancy pump. At this point, the autopilot is turned off and the vehicle is brought to a horizontal attitude to minimize sinking during the time (approx. 10 min.) that the pump brings the vehicle to its net ascent buoyancy. The vehicle is then pitched up and the autopilot turned on for ascent.

The glider successfully performed several controlled ascent/descent cycles before a pump problem precluded controlled ascents on the last two days of testing. The depth of controlled dives ranged between 100 and 300 feet.

II. DATA PRESENTATION AND DISCUSSION

This section presents the predicted and measured performance results of each glider model and its field trials. The presentation for each glider model is immediately followed by a discussion of the results and their effect on the design of the next model.

Predicted and actual measured performance results are graphically presented in the following manner:

Gliding Performance: A plot of vehicle speed along the glide path vs. glide angle was deemed the best indicator of gliding performance. It not only shows the effects of drag for different models or different features of the same model (such as different size wings), but serves as an indicator of the "robustness" of the vehicle's gliding ability. The vehicle will probably be operating at a pitch angle that maximizes its horizontal speed, typically 40-50°. However, the vehicle should be capable of effective gliding over a wider range of pitch angles that may be encountered over time. These could be corrected by appropriate longitudinal adjustment of the moveable weight but at an energy cost and decreased vehicle scientific life. An example of this is the coupled change in pitch angle when the vehicle is rolled to perform a steering action. Glide path speed was inferred from an internally logged record of depth vs. time, pitch angle as well as analytical knowledge of angle of attack vs. pitch angle.

Turning Performance: A plot of steady state turning rate vs. wing bank angle is used as the primary indicator of turning performance. It not only gives the autopilot designer critical information about vehicle steering characteristics but also serves to point out the likely magnitudes of the inevitable asymmetries between right turn/left turn and ascent/descent modes that must be eventually dealt with through design or compensation.

Plots of steady state turning radius as function of wing bank angle are also presented. Since the actual turning rates are relatively small, turning radius is given as a performance indicator that is easily visualized and understood physically.

Autopilot Performance: Autopilot performance is presented as the raw data of heading angle vs. time in the controlled mode for a range of tested off-course errors and feedback gain settings. Some selected predicted simulations are also given.

Other Data: Some selected examples of specific cases of unreduced raw data output are shown to illustrate specific features important in the discussion of results.

Computer Simulated Predictions: All examples of predicted vehicle performance either utilize inputs from or are direct outputs of a unique, computer-simulated model of the vehicle. It is a 6 DOF, non-linear model, with accommodation for a wide range of vehicle maneuver and disturbance inputs. It is mechanized on the TUTSIM-6 Block Diagram Simulation Language for use on a personal computer (Ref. 2).

1. PROTOTYPE GLIDER

A. Data Presentation

a *Gliding Performance:* Actual glidepath speed as a function of pitch angle is given in Figures 7, 8, and 9 for all three wing sizes used in the prototype model. The predicted speed curve is given for the medium wings. The pool test stall results are also included in these plots as the zero speed limits.

b. *Turning Performance*: Plots of actual steady state turn rate as a function of wing bank angle are shown in Figures 10 and 11. A comparison with predicted values is given in Figure 12 for the medium wings. Actual turning radii for the medium wing size is presented in Figure 13.

c. *Other Data*: Representative raw data plots of pitch angle vs. time for the small and medium size wings are given in Figures 14 and 15. These serve to illustrate the presence and magnitude of observed vehicle pitch oscillations in the steady gliding mode after the initial down/up transient. A plot of heading angle as a function of time, for the dive shown in Figure 15 with the wings at -23° deflection, is shown in Figure 16. This clearly shows the presence of heading oscillations at the same time as the pitch oscillations of Figure 15. A plot of wing angle vs. time is shown in Figure 17. This shows roll oscillations coupled with those in pitch.

B. Discussion of Results

a. *Gliding Performance*: Figure 8 shows good agreement of actual with predicted glide speed in the pitch angle range where an analytical gliding solution is provided by the computer model. The few points for the medium wings at lower pitch angles, including the stall angle of 8°, appear to lie roughly along a line projected back from the predicted solution line. This effect is more clearly seen in Figure 7 for the small wings where more dives were made at the smaller pitch angles. It should also be noticed that the small wings showed an approximately 20% speed increase over the medium wings at pitch angles greater than 35° due to decrease in direct and induced drag. Figure 9 for the large wing set shows glide speed performance essentially similar to that of the medium wings.

Two major conclusions may be drawn from the gliding performance curves. First, glide speed is reasonably predictable using the computer model. Second, some semblance of gliding, although at large angles of attack, seems to be

able to be initiated right down to stall pitch angles of 5°-10° with the horizontal. Although operation of the vehicle at low pitch angles is not intended, degradation or changes in either the vehicle's hydrodynamic, control or drive characteristics over long missions could sometimes find it operating at lower than intended pitch angles. Also, the vehicle must be capable of transiently operating from near horizontal to its optimal pitch angle (approx. 45°) upon initial sinking at each dive initiation from its nose-up, surface orientation, and also upon turn-around at depth.

On first inspection, it seems that the small wings would be the preferred set due to the greater glide speed obtained with them. However, other considerations explained below, such as turning performance and stability, led to the adoption of the area of the medium size set for the subsequent lake model.

b. Turning Performance: Steady state turn rate for all three wing sizes in Figures 10 and 11 show somewhat asymmetric and inconsistent results for the small and large wing sets with respect to both ascent/descent and right/left wing bank angles.

The plots for the medium wings show little asymmetry or offset. This can be seen more clearly in Figure 12 where the medium wing results are plotted along with predicted turn rates from the computer simulation. These show very good agreement between actual and simulated results at the higher wing bank angles whereas the simulation generally underestimates actual performance at wing angles less than 15°.

Figure 13 shows actual turn radius as a function of wing bank angle for the medium wings. The original target of a 50-100 m turn radius is well met at bank angles even as small as 5°, with a 25° bank producing a very tight 21 m radius. This has very positive implications for using minimum energy in long term deployments, since the actuation motors that cause the vehicle (and hence the rigidly attached wings) to roll will not have to be moved very far to achieve acceptable turning.

c. Other Data: Figure 14 shows vehicle pitch oscillations of ±5° during descent and ±9° during ascent after the abrupt turnaround transient following the drop of the nose weight. Figure 15 shows a similar plot for a dive with the medium wing set where reduced pitch oscillations of ±1.7° and ±5° are observed for descent and ascent respectively. This reflects the increased added mass of the medium wings, an effect that was exploited further in the lake test glider.

Figure 16 shows typically observed heading oscillations during both the ascent and descent portions of the dive shown in Figure 15. Although an average steady turn rate was always observed, efforts were made to suppress the oscillations of this probably unstable mode in the lake test model. The cause of the oscillations is suspected to be hysteretic wing stalling due to separation of the flow at the leading edges of the wings. The triggering mechanism for this appears to be pitch oscillations occurring at the same time as those observed for heading (see Figures 15, 16). This is further confirmed by Figure 17, which shows wing bank angle as a function of time for the same dive. This shows coupled wing angle oscillations of up to 4° about the -23° (left) set bank angle, occurring at the same times (approx. 40, 80, 200 and 240 sec) as the pitch oscillations. A goal for the lake test unit was to decrease induced disturbances on the vehicle and reduce the wings' sensitivity to low speed separation.

d. Design Improvements: The following design improvements were made in the lake test model glider in light of the results described above for the prototype.

1. Increasing Glide Speed

Increases in glide speed were anticipated in the lake test glider by increasing the net drive to 50 g and by reducing drag. The latter is accomplished by careful attention to forward and aft fairing design and to wing drag reduction through wing configuration and attachment improvements.

2. Decreasing Pitch Oscillations

Pitch oscillations can be reduced by decreasing the pitching moment of the vehicle. However, it was desired to accomplish this without changing the lift and hence the turning force available for steering. This was done in the lake test unit by changing from a box wing configuration to an equivalent lift cruciform with the four wings bolted directly to the thermal engine housing (see Figure 4). With both main lifting wings now directly exposed to cross-flow, instead of shielding one another as in the box wing configuration, their effective added mass, and hence resistance to pitch accelerations, was increased by 76% with little change in lift.

3. Increasing Turn Rate

Although the turning rates and radii obtained in the prototype unit with the medium wing set were well within desired target of 100 m, it was desirable to improve on the lake test model by providing a greater safety margin over the vehicle's deployed life and to possibly minimize the energy required for turning maneuvers. To accomplish this without increasing the size of the lifting wings, it was necessary to increase the asymmetry ratio of the horizontal to vertical wings. A further requirement was to avoid significantly decreasing the effective lateral stability of the vertical wings.

These improvements were accomplished by placing the cruciform wingset of the lake test glider on the outside of the thermal engine housing. This places an identical portion of each wing's area near the root chord attachment point in the trailing wake of the aft conical fairing during normal forward motion; thereby decreasing each wing's effective area by the same amount. However, since there is a difference in area between the horizontal and vertical wings, the decrease in effective area increases the asymmetry ratio without changing actual wing areas. The vertical wings are still fully exposed to, and can resist large angle of attack lateral crossflows, hence preserving the good lateral stability of the original boxwing. The lake test model has an effective asymmetry ratio increase of 90% over the prototype, while essentially preserving the stability characteristics of the medium size box wing.

4. Increasing Wing Low Speed Stall Resistance

The prototype box wings were designed with a conventional section of a rounded leading edge tapering to a sharp trailing edge. Research into the sparsely studied area of wing performance at the low operating Reynolds numbers of the wing (typ. 25,000) revealed that flow separation can occur from a rounded leading edge at an angle of attack. Review with our hydrodynamic consultant (H. Jex, STI Corp., Hawthorne, CA), one of the few experts in low Reynolds number wing performance, led to the adoption of a wing section with a sharp, tapered leading edge.

5. Improving Vehicle Configuration

The physical configuration of the prototype glider was changed in two significant ways to make it more compatible with long-term ocean deployment.

a. The platform of the wings was changed from rectangular to swept to promote weed/trash shedding.

b. The antenna mount was shifted to the nose for internal packaging purposes and to keep the wings below the air interface when the vehicle is in the vertical, satellite transmission mode at the surface. The objective was to minimize both stress on the wings from wave action and any tendency for the wings to collect and trap weeds while at the surface, or during the initial phases of sinking at dive initiation.

2. LAKE TEST GLIDER

A. Data Presentation

a. Gliding Performance: Predicted and actual glidepath speed as a function of pitch angle is shown in Figure 18 for both the Raytheon tank tests and the Seneca lake trials, each run at ±50 g net drive.

b. Turning Performance: A plot of predicted and actual steady state turn rate as a function of wing bank angle is given in Figure 19. Actual turning radii are presented in Figure 20.

c. Other Data: Raw data plots of pitch angle and heading as a function of time are shown in Figures 21 and 22 respectively. These figures illustrate the complete absence of pitch and heading oscillations in the lake test glider.

d. Autopilot Performance: Several plots of heading angle as a function of time under autopilot control are given in Figures 23, 25 and 26 for various values of initial heading error and autopilot gain. Comparison with predicted performance is also presented for dives 7 and 9 in Figures 23 and 25. Dive 7 was performed at a value of autopilot gain considered to be near optimal from the pre-test computer simulations. Figure 24 is a time history of the wing bank angle for dive 7.

B. Discussion of Results

a. Gliding Performance: Figure 18 shows the actual lake model glide speeds in good agreement with predicted values, with a nominal 52% increase over that of the prototype at 40° pitch angle. This is considerably greater than the 13% increase expected from a straight scale-up by the square root of the ratio of their net drive forces (50 g, 39 g respectively). This implies that the goal of considerable drag reduction has been met and that a reduction of 44% in the effective drag coefficient has been achieved.

Figure 18 also shows maintenance of a reasonable glide speed in the region below 35° pitch angle where analytical predictions are not obtained. Data points there project back from the predictable region in a reasonably smooth fashion. This would seem to indicate that operation at low pitch angles remains stable and maintains the goal of gliding "robustness" to off-design operating points or to near-optimal points for which energy expenditure to continuously correct may not be justified.

b. Turning Performance: Figure 19 shows an average of steady state turn rates for the lake test glider over several runs at the same wing bank angles. The rates are generally 300-400% higher than comparable ones for the prototype with the medium wings. This indicates that the vehicle speed increase and the increase in the horizontal/vertical wing asymmetry ratio has been effective in significantly increasing turning performance. Predicted values generally understate actual ones at lower wing angles, as was the case with the prototype model. This, again, is a positive implication for potential energy minimization goals, and can be fairly easily adjusted for in the predictive computer models.

Figure 20 shows that the turn radii for the lake test model were reduced significantly (70-80%) from the medium wing size prototype for the same wing bank angles. In addition, the curve is much flatter from low to high bank angles, reflecting the relatively high turn rates observed at low bank angles (see Figure 19) in the lake test model.

c. Other Data: Figure 21 shows a time plot of pitch angle for the descent phase of one of the autopilot dives at Seneca Lake. The descent pitch angle of -49° (nose down) is solidly maintained, with no evidence of the large scale 25-50 sec pitch oscillations seen in the prototype. The high frequency .5° noise seen in the record is 1 count jitter in the A/D converter of the vehicle data logger. This was also seen in the prototype trials (Figures 14, 15).

Figure 22 is a time plot of heading angle for one of the ascents made in the Raytheon test tank. A test tank run was chosen for illustration since the wing angle is fixed (here 34° right bank) and steady-state turning is quickly reached as opposed to the lake autopilot runs where the wing setting is constantly changing. The plot is seen to be smooth with no evidence of the heading reversals seen in the prototype. The flat, slightly jagged portion in the first 15 seconds of the run is during the pitch-up of the vehicle from its initial horizontal position on the tank bottom, prior to the commencement of any forward gliding motion. The withdrawal of the bottom holding device at the beginning of this initial righting almost always induced some small heading perturbation during the static pitch-up.

d. Autopilot Performance: Figure 23 shows the glider, under autopilot control, correcting an initial heading error of 42° in 80 seconds, and holding course within ±2.5° thereafter. This compares very well with the predicted values over most of the plot. The actual performance showed slight hunting about the control heading, whereas the simulation at the same gain, predicted a smooth, overdamped asymptote to the control heading. This is explained by the fact that the vehicle data logger, which also served as the overall controller, was not capable of floating point arithmetic. It was therefore not capable of producing a corrective signal once the feedback variables dropped below certain minimums, typically near the control point. At these times the algorithm would stop corrective action at the last wing setting until a large enough (typically overshot) error was detected, or it would put the wings to the horizontal position if corrective action was not called for after a certain wait period. This artifact produced flat spots in the wing deflection curve, at or near the horizontal wing position, when the vehicle was near the control point. This action is evident from Figure 24, the wing angle time history for this run. This effect will not be present at all in the ocean model with its higher level controller and in no real way detracts from the success of the control algorithm's performance. In fact, the ±2.5° overshoots seem remarkably small given the crude nature of the corrective action near the control point and are not important relative to long-term ocean deployment where control action decision deadbands will be large (typ. ±30°).

Figure 25 shows the results of autopilot dive 9 which was a controlled run at an autopilot gain of half that of dive 7 (Figure 23). It shows excellent agreement with predicted values over most of the corrective action range but with faster movement of the actual vehicle toward the set heading in the later stage of control. This is entirely explained by the results shown in Figure 19, where the actual turn rates of the vehicle at wing angles less than 10° are seen to be greater than five times those predicted. The wing angle during dive 9 (Figure 25) is less than 8° for time greater than 60 seconds, so faster than predicted performance is not surprising.

Figure 26 is for a dive with an autopilot gain intermediate between those of the two previously discussed runs, which were the high and low points respectively of the tested gain range. It shows performance very similar to that of dive 7 (Figure 23) with respect to the corrective maneuver and subsequent course keeping, and is presented without further discussion.

e. Design Improvements: The following design improvements are intended for the first ocean demonstration model in light of the results described above for the lake test model.

1. Increased Glide Speed

The glide speed of the lake test glider was increased over that of the prototype largely through drag reduction, with some contribution from increased drive force. Significant further drag reductions are not likely, so a glide speed increase for the ocean glider will come from increased drive. The drive force for the ocean test model will be increased to ±100 g with an expected glide path speed of .44 m/sec (.28 m/sec horizontal). This is more in line with speeds originally deemed necessary in order for the SLOCUM vehicle to perform meaningful station-keeping in the ocean.

2. Buoyancy Compensation

The SLOCUM vehicle's sawtooth depth profile and fixed buoyancy change imply that its forward progress over the bottom is maximized by maintaining the dive angle that results in maximum horizontal velocity and by maintaining the constant drive force over the course of the dive. The latter can only happen if the vehicle's total compressibility and thermal expansion match those of the ocean. Without compensation, the vehicle with 100 g negative buoyancy at the surface would become lighter as it dived and reached equilibrium at about 1000 m. The ocean test glider will employ passive buoyancy compensators to closely match the vehicle's density variation to that of the ocean over its entire 1800 m operating range.

3. Revise Autopilot Simulation

The autopilot simulation program for the ocean glider will be revised to reflect the observed increased vehicle turning performance relative to that predicted at the lower wing bank angles. This will enable the autopilot gain to be optimized in a way that minimizes energy use by the vehicle roll actuator.

III. OCEAN TEST GLIDER PLANNING

The successful results of the described glider trials and separate lab and field trials of a thermal buoyancy change device have led to the following specifications for an ocean glider unit.

Specifications

Physical Configuration and Size: Same as Lake Test Glider
Collapse Depth: 3000 m
Hull Material: 7075-T6 aluminum
Energy Consumption: 1 Wh/day
Endurance: 5 years
Buoyancy Change: ±100 g about neutral
Additional Surface Buoyancy: 700 g
Nominal Glide Speeds: 0.33 m/sec (vertical)
0.28 m/sec (horizontal)
Design Turn-Around Depth: 1800 m
Nominal Operating Temperature Difference: 15°C (surface-1800 m)
Autopilot Sample Interval: 60-120 sec (est.)
Satellite Communication: ARGOS
Data Sensors: Temperature, depth (demonstration unit); CTD, current meter, other sensors (follow-on science units)
Navigation: Dead-reckoning autopilot; pre-programmed headings (demonstration unit); custom GPS navigation module (target)

It is expected that the first ocean demonstration glider would essentially be the same physical size as the lake test unit but with active drive and surface buoyancy thermal engines. The autopilot would simply steer a pre-programmed triangular or rectangular course. Depth and temperature data would be measured on one or more descents per day and transmitted via ARGOS daily. The position of the unit at the surface as well as science and engineering data would be received from the ARGOS transmission.

A successful field trial of the ocean glider would lead to the fabrication and testing of two more with full science and navigation packages. Gliders like this, with various sensor configurations, could then become available for use by the scientific community.

IV. SUMMARY AND CONCLUSIONS

Two design iterations toward the utlimate goal of a SLOCUM glider capable of long-endurance profiling missions to the interior of the ocean as part of a large-scale ocean observational system (Ref. 1) have been completed. The significant accomplishments and conclusions of the work are the following:

1) A basic glider configuration which is dynamically stable, minimizes drag and anticipates future system packaging and mission needs has been evolved and tested.

2) Drag reduction has been accomplished to the extent that the target horizontal speed of .5 knot can be obtained by simply increasing the net gravitational drive force to 100 g.

3) The greatly simplifying concept of utilizing an internal weight shift to accomplish pitch attitude and turning maneuvers has been very successful. Turn radii ten times less than the 100 m originally estimated as acceptable have been obtained with reasonably sized, rigidly-attached wings.

4) Performance-robbing and potentially unstable pitch and heading oscillations observed in the first prototype glider have been completely eliminated by a new wing configuration and section design. The new configuration also has the benefits of greatly reduced drag and enhanced weed/trash shedding properties due to its swept platform.

5) A unique, computer-simulated model of the SLOCUM glider has been developed and mechanized on a PC. It has proven accurate in most aspects of predicted performance with all significant discrepancies being on the side of performance underprediction.

6) An extremely simple heading autopilot seems capable of controlling vehicle heading to about ten times the accuracy that will likely be needed in eventual long-term ocean deployments. This same algorithm has been successfully employed in computer simulations of ocean mission situations with autopilot update intervals up to 60 times longer than those employed in the lake tests.

In conclusion, the originally most risk-prone aspect of the SLOCUM concept: an autonomous, near-neutrally buoyant glider, has been proven largely successful. Subsystem designs such as effective realization of the thermocline-driven buoyancy change engine and low-power 2-way satellite communication are now the controlling factors in long-term system success.

V. ACKNOWLEDGMENTS

Funds were provided to Webb Research Corporation under subcontract to the Woods Hole Oceanographic Institution through ONT Contract No. N00014-90-C-0098. Guidance and encouragement provided by WHOI principal investigators Dr. Philip Richardson and the late Dr. Henry Stommel are gratefully acknowledged. Special recognition also goes to Douglas Webb and Dr. Joshua Hoyt of Webb Research Corp. for the original SLOCUM glider and weight-shift mechanism designs, and to Henry Jex of Systems Technology, Inc. for the computer simulation model.

VI. REFERENCES

1. Henry Stommel, The SLOCUM Mission, Oceanography, April 1989, 22-25.

2. Henry R. Jex and Keith J. Owens, 1991. The SLOSIM Simulation Program Guide. Systems Technology, Inc., Working Paper No. 2398-7.

SLOCUM - OPERATIONS PROFILE

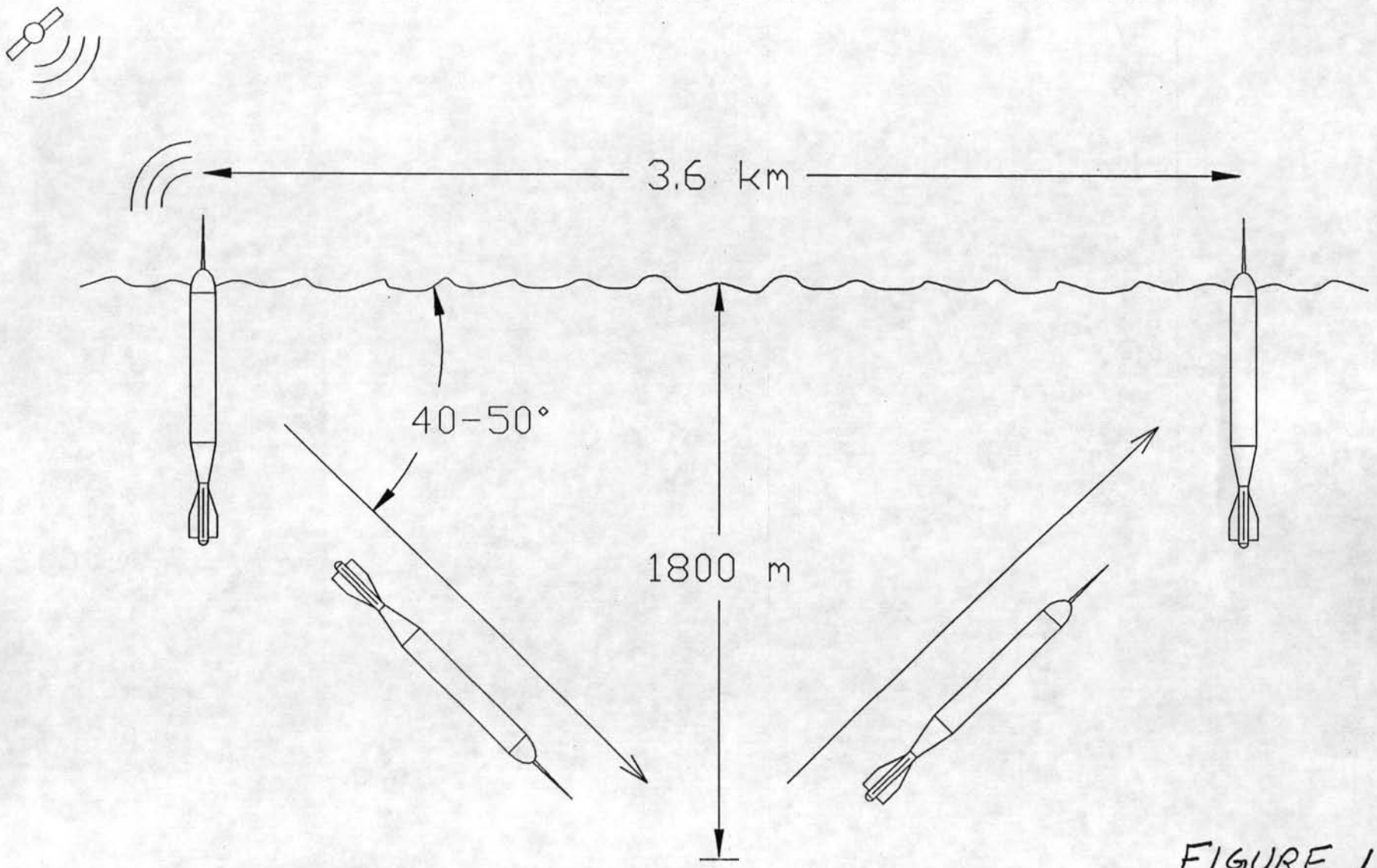

FIGURE 1

Average Horizontal Speed Approx. 28 cm/sec. →

An AUV of 5 years and 40,000 km autonomy
Two way satellite communications and positions from GPS
During dive vehicle is under autopilot control while taking observations

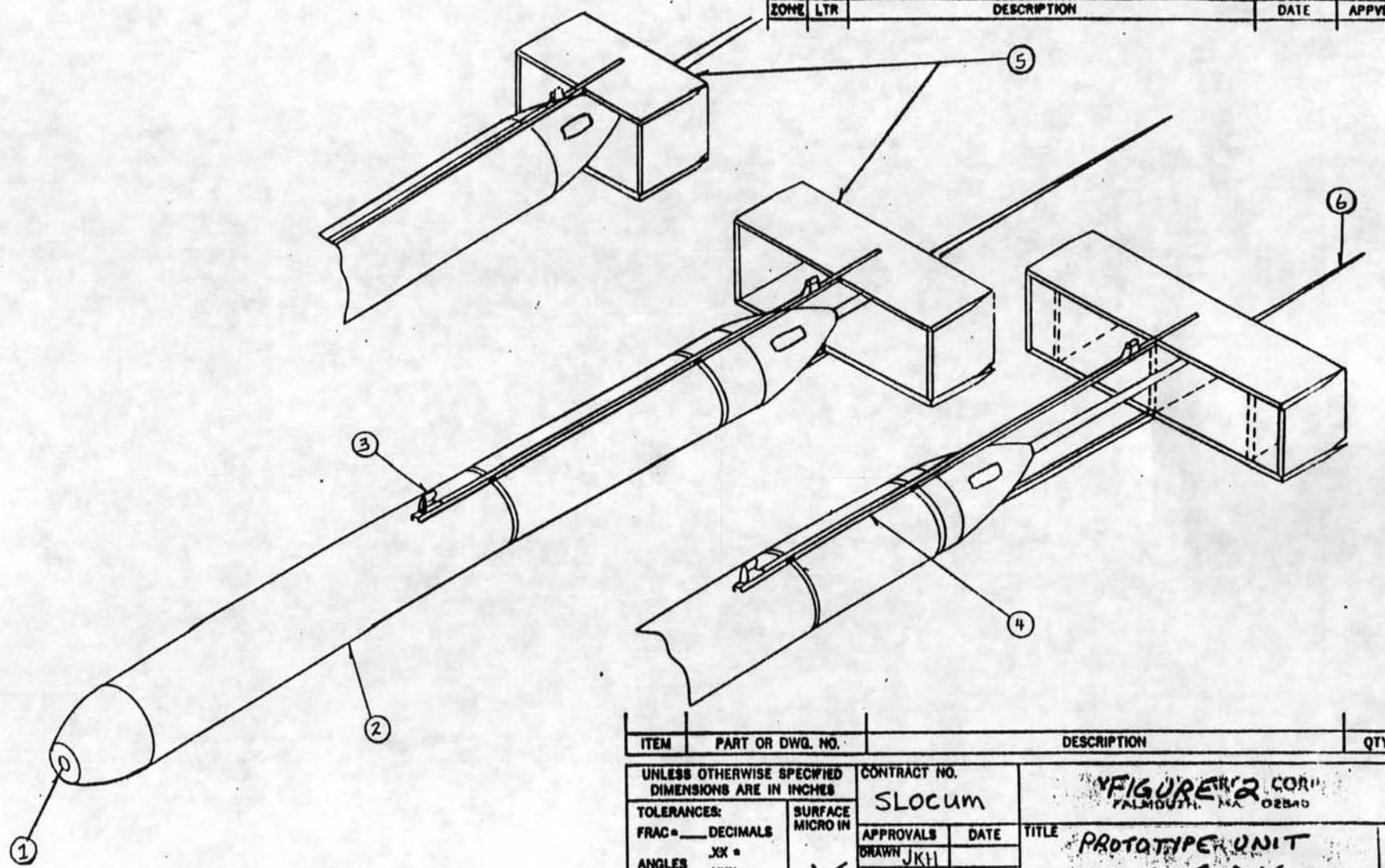

REVISIONS				
ZONE	LTR	DESCRIPTION	DATE	APPVD

ITEM	PART OR DWG. NO.	DESCRIPTION	QTY

UNLESS OTHERWISE SPECIFIED DIMENSIONS ARE IN INCHES

TOLERANCES:
FRAC ± ____ DECIMALS
ANGLES ° .XX ± .XXX ±

SURFACE MICRO IN ✓

MATERIAL

CONTRACT NO. SLOCUM

APPROVALS	DATE
DRAWN JKH	
CHK'D	
APPVD	
FINISH	

FIGURE 2 CORP
FALMOUTH, MA 02540

TITLE PROTOTYPE UNIT OUTLINE DWG.

SIZE | DWG. NO. | REV.

SCALE | SHEET OF

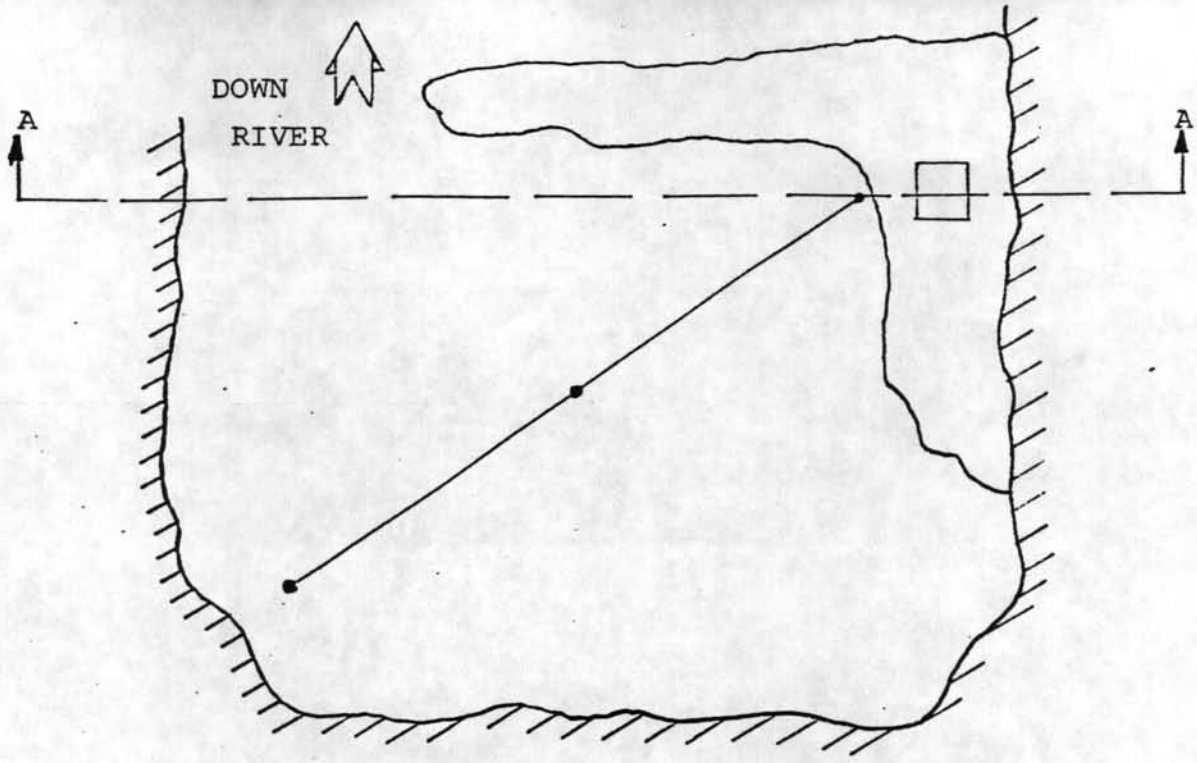

BIRD'S EYE VIEW

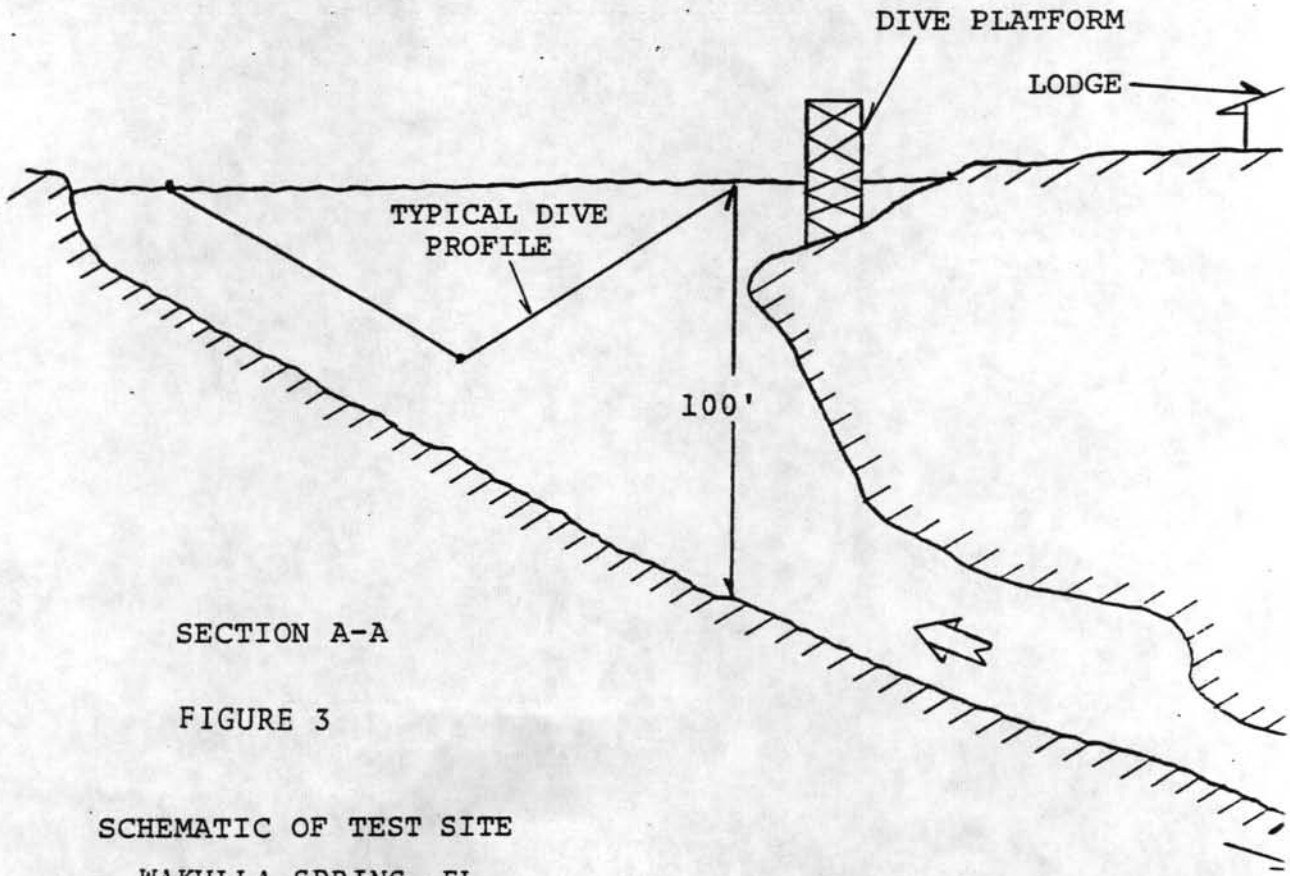

SECTION A-A

FIGURE 3

SCHEMATIC OF TEST SITE
WAKULLA SPRING, FL

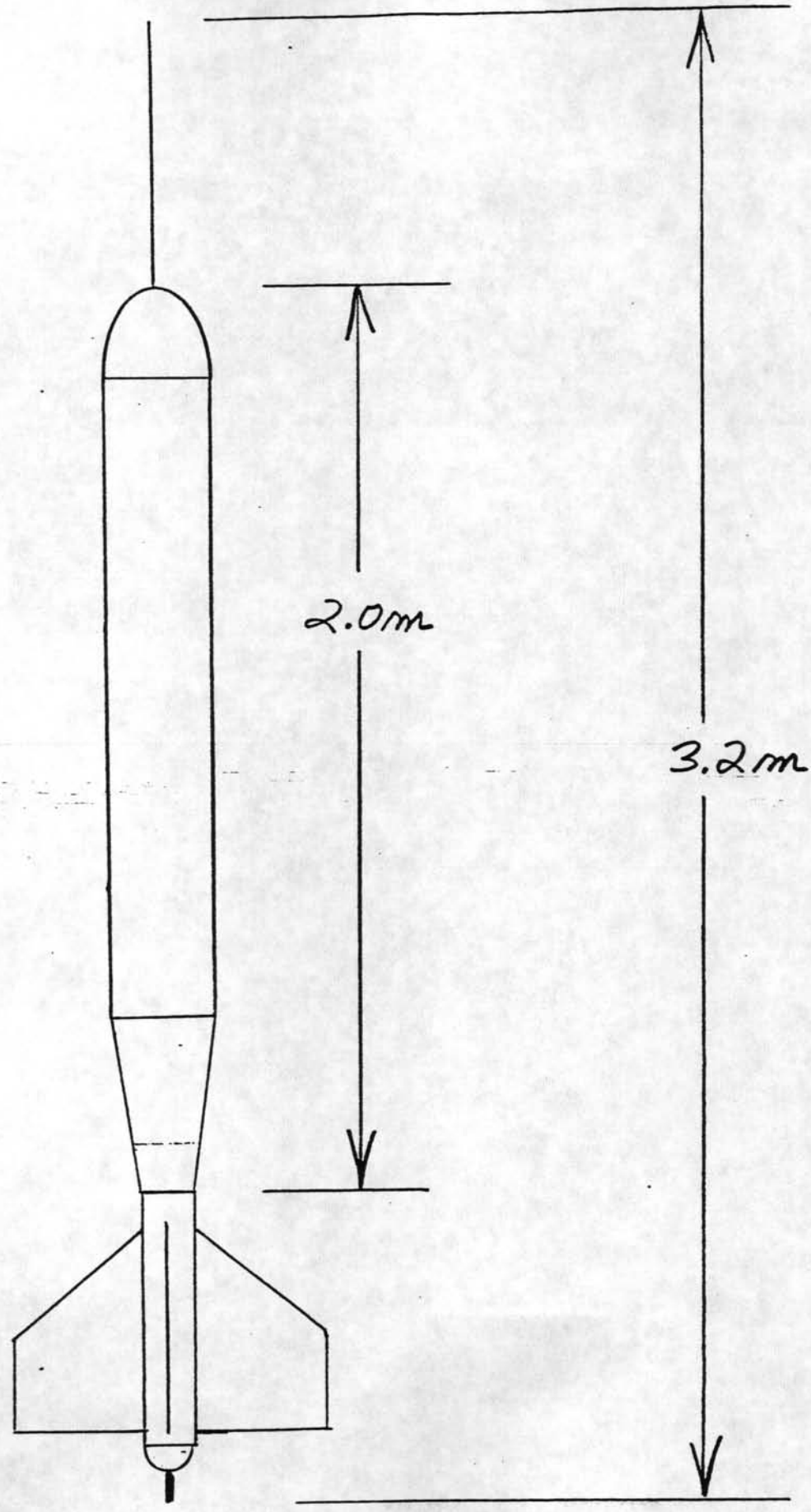

FIGURE 4 LAKE TEST GLIDER UNIT OUTLINE DWG.

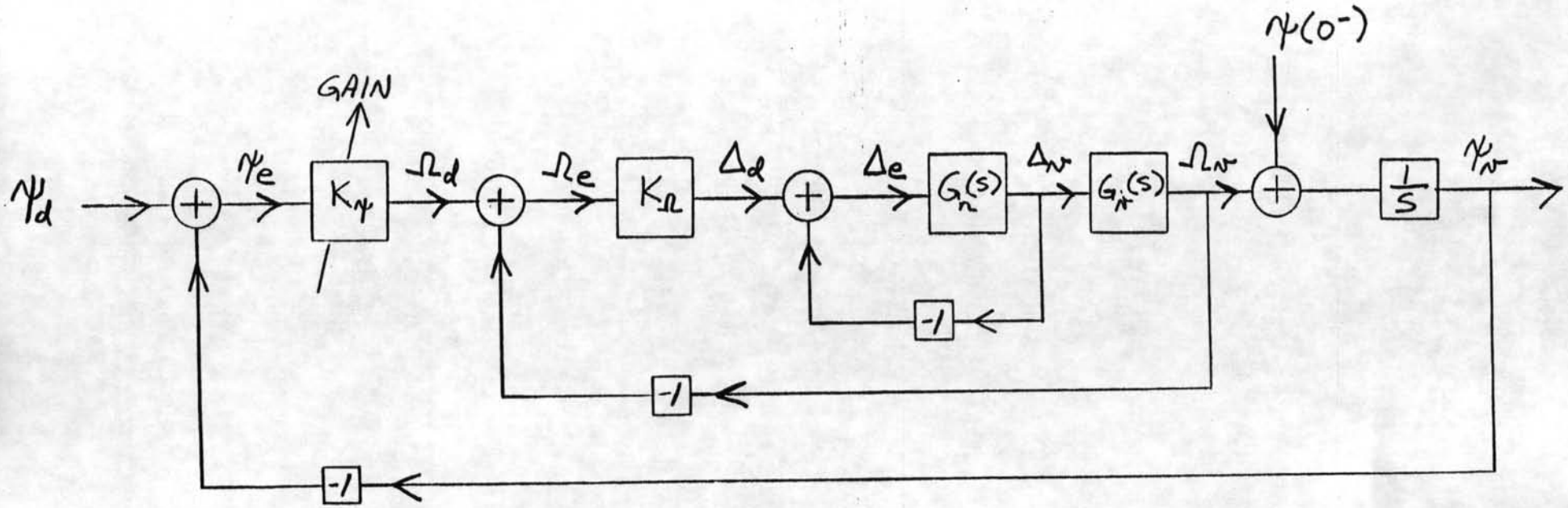

NOMENCLATURE:

PHYSICAL VARIABLES

ψ = Heading Angle

Ω = Heading Rate

Δ = Roll Deflection

FEEDBACK VARIABLES

K_i = Feedback Constant

$G_i(s)$ = Transfer Function

s = Laplace Transform Argument

SUBSCRIPTS

d = desired

e = error

v = vehicle (actual)

r = roll actuator

FIGURE 5: HEADING AUTOPILOT BLOCK DIAGRAM

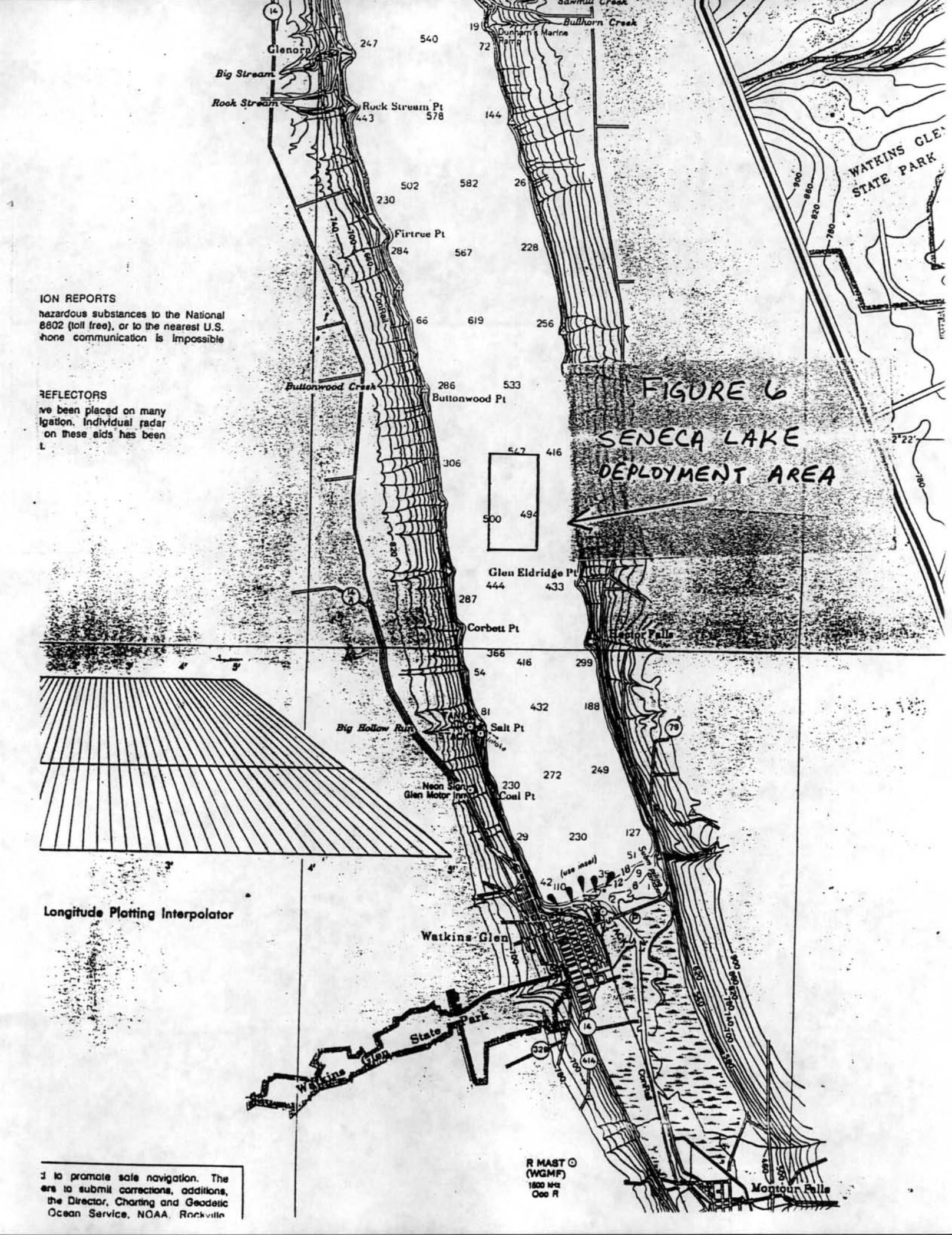
ION REPORTS
hazardous substances to the National
8802 (toll free), or to the nearest U.S.
hone communication is impossible
REFLECTORS
ve been placed on many
igation. Individual radar
on these aids has been
t.
FIGURE 6
SENECA LAKE
DEPLOYMENT AREA
Glenora
Big Stream
Rock Stream
Rock Stream Pt
Dunham's Marina
Bullhorn Creek
Sawmill Creek
Firtree Pt
Buttonwood Creek
Buttonwood Pt
Glen Eldridge Pt
Corbett Pt
Harbor Falls
Big Hollow Run
Salt Pt
Neon Sign
Glen Motor Inn
Coal Pt
Longitude Plotting Interpolator
Watkins Glen
State Park
WATKINS GLE
STATE PARK
R MAST
(WGMF)
1600 kHz
Montour Falls
ed to promote safe navigation. The
ers to submit corrections, additions,
the Director, Charting and Geodetic
Ocean Service, NOAA, Rockville

FIG.7 (SMALL WINGS)
GLIDE SPEED VS PITCH ANGLE

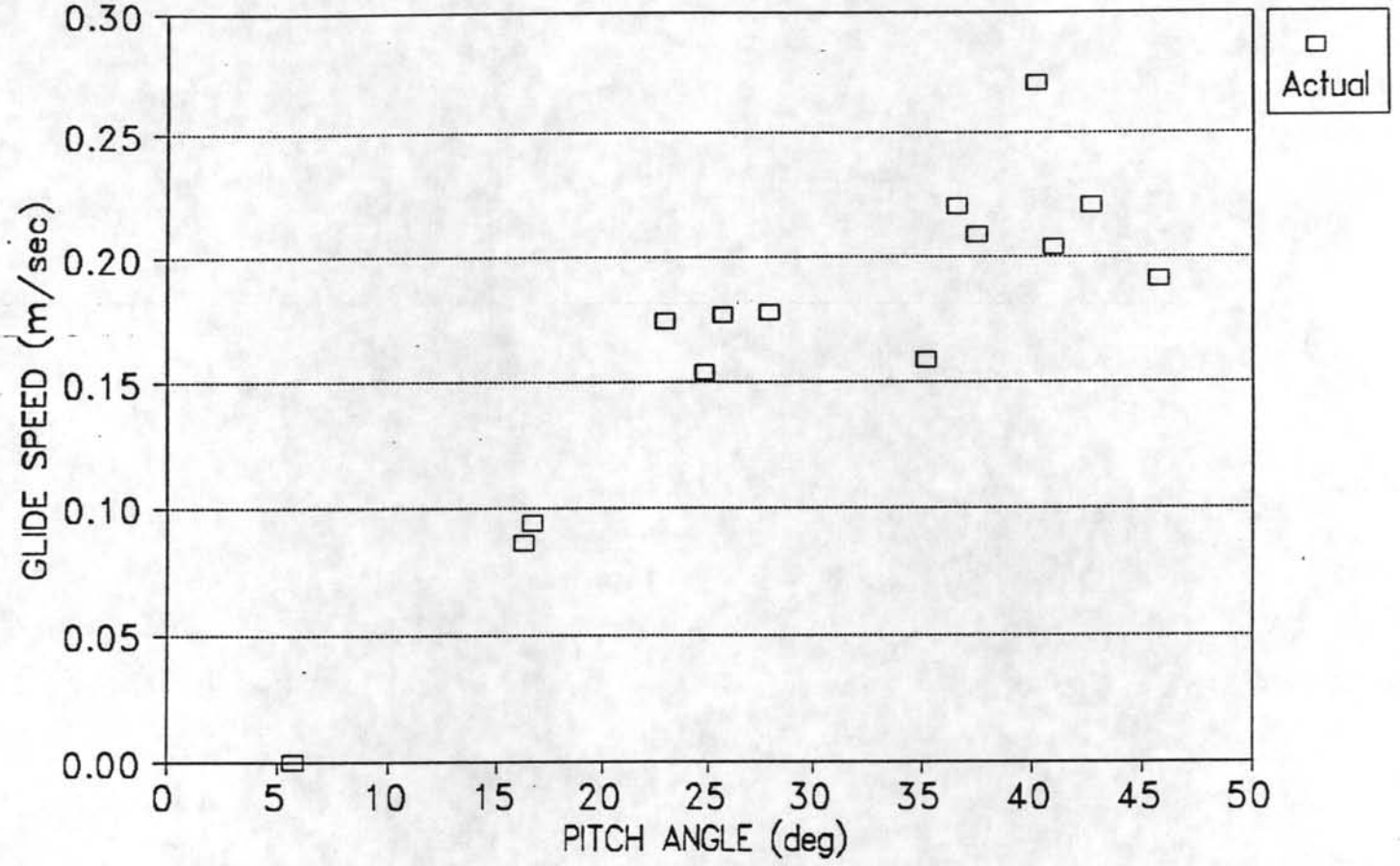

FIG.8 (MEDIUM WINGS)
GLIDE SPEED VS PITCH ANGLE

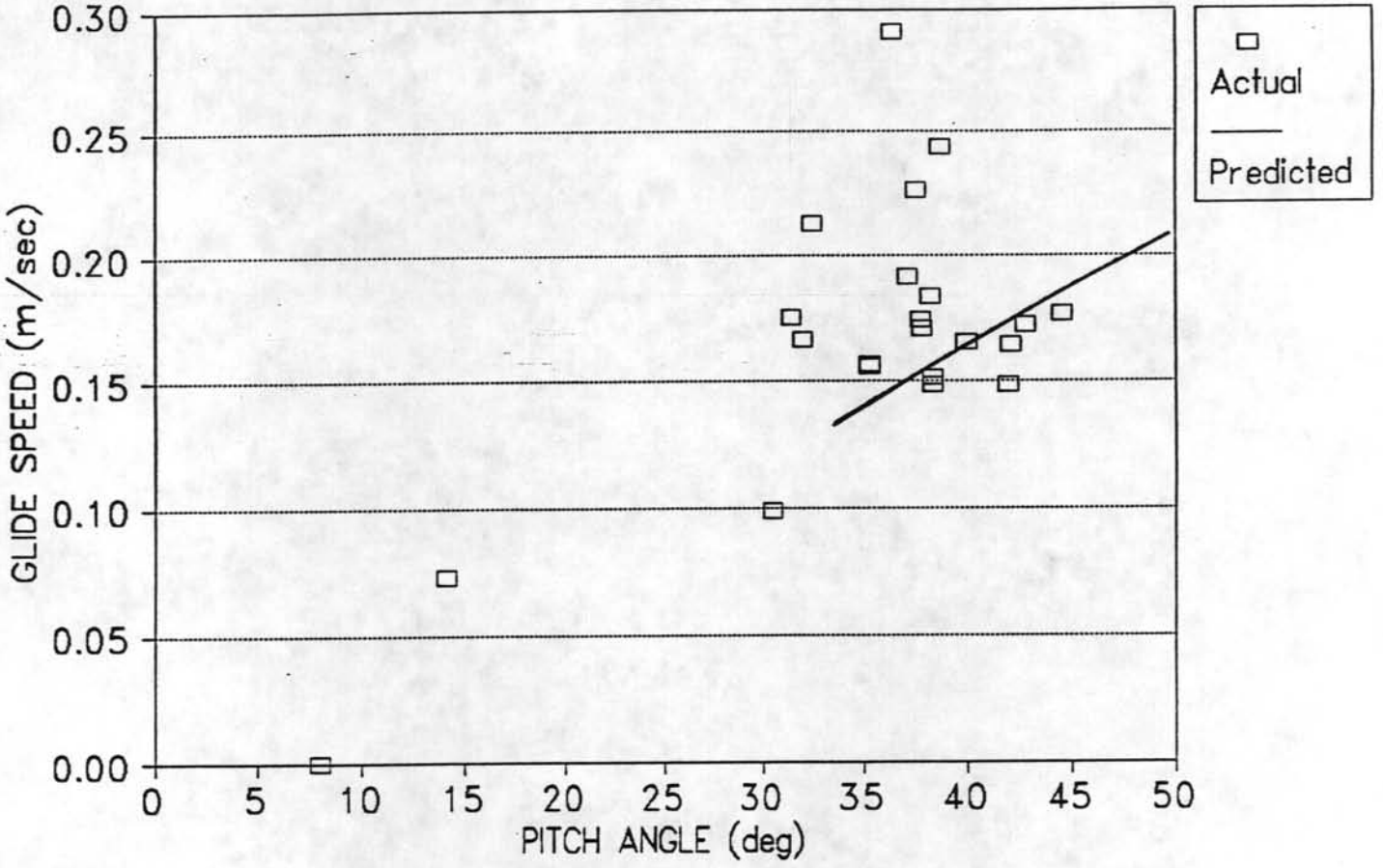

FIG.9 (LARGE WINGS)
GLIDE SPEED VS PITCH ANGLE

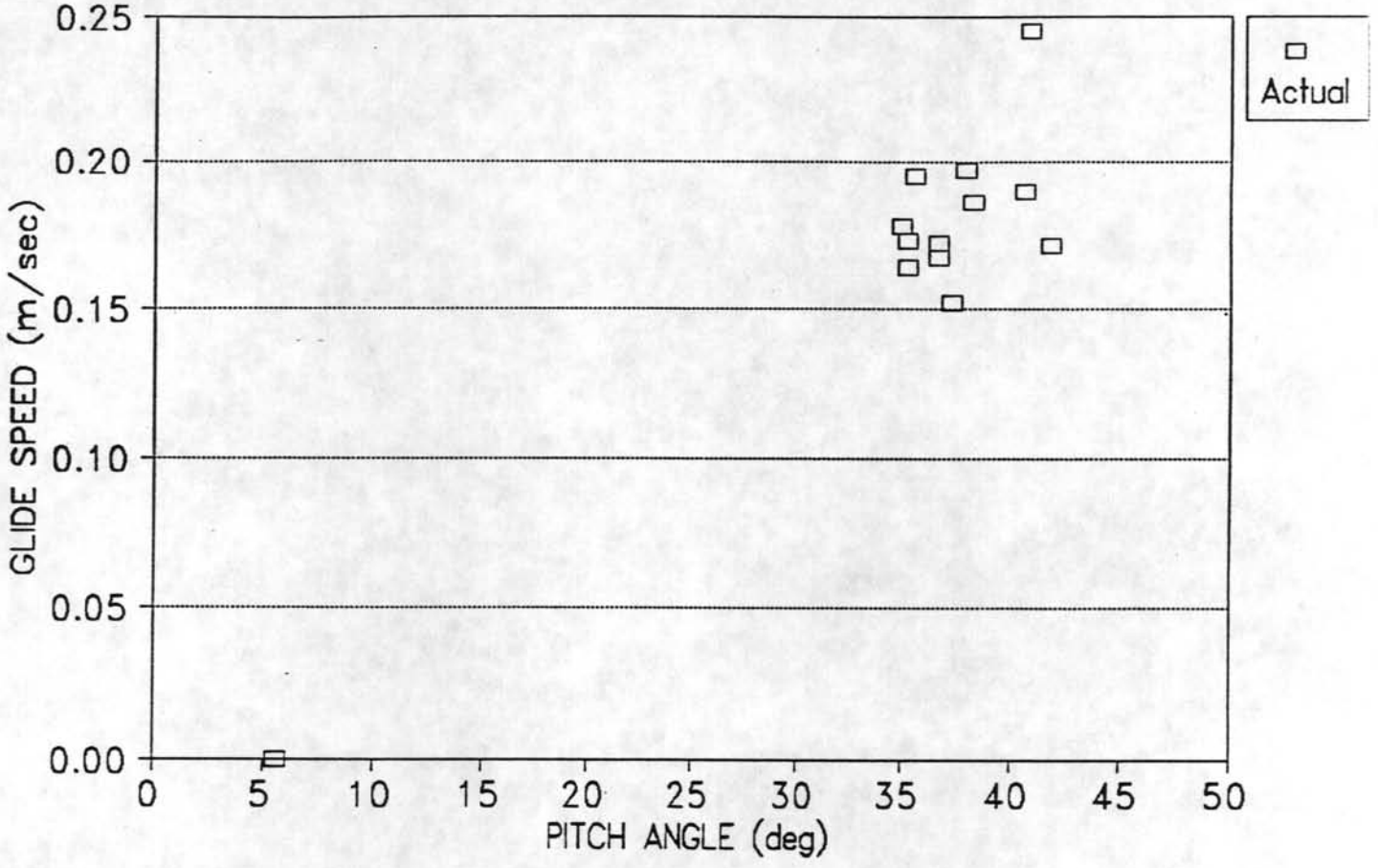

FIG.10 (ASCENT, ALL WINGS)
S.S.HEADING RATE VS BANK ANGLE

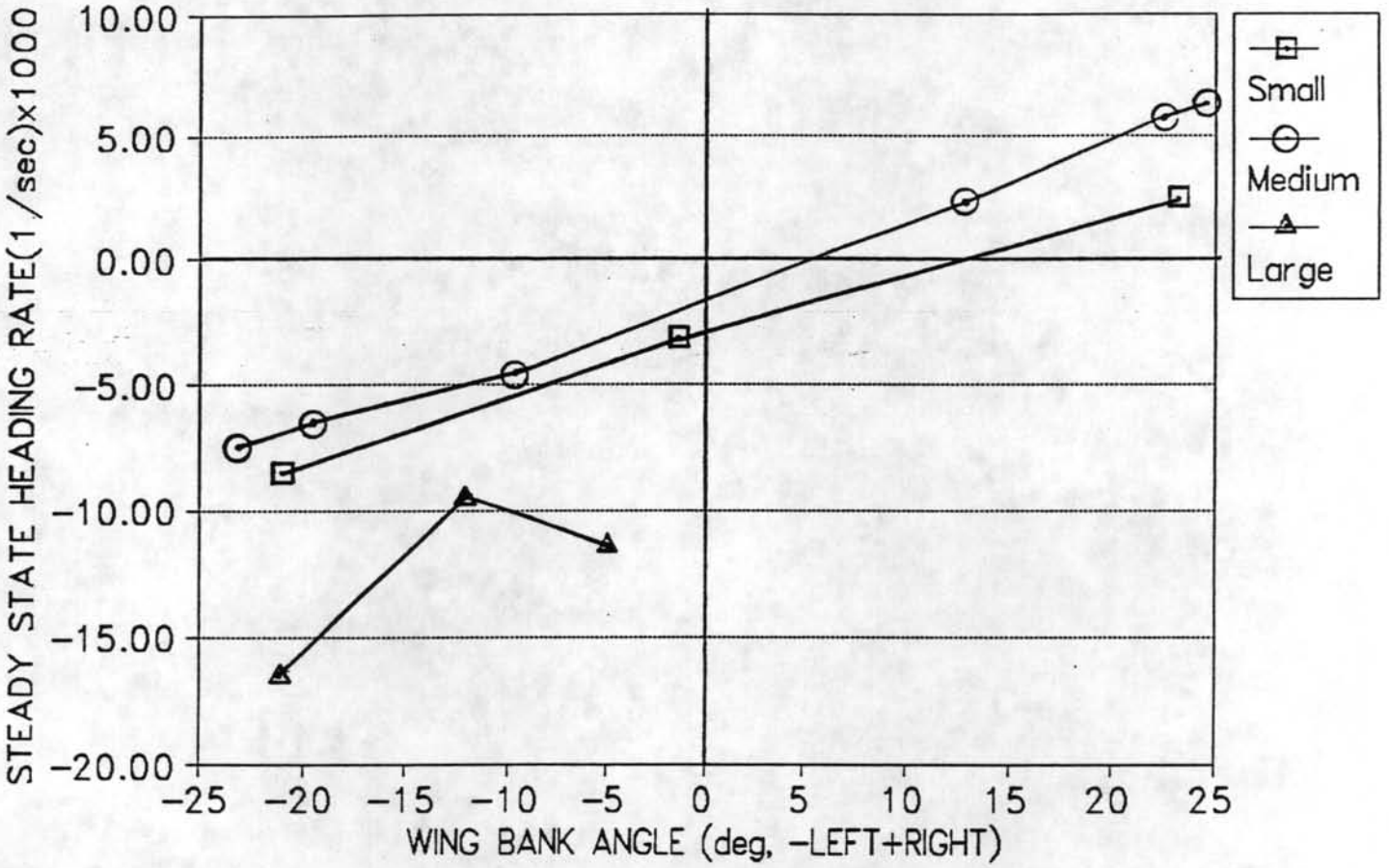

FIG. 11 (DESCENT, ALL WINGS)
S.S.HEADING RATE VS BANK ANGLE

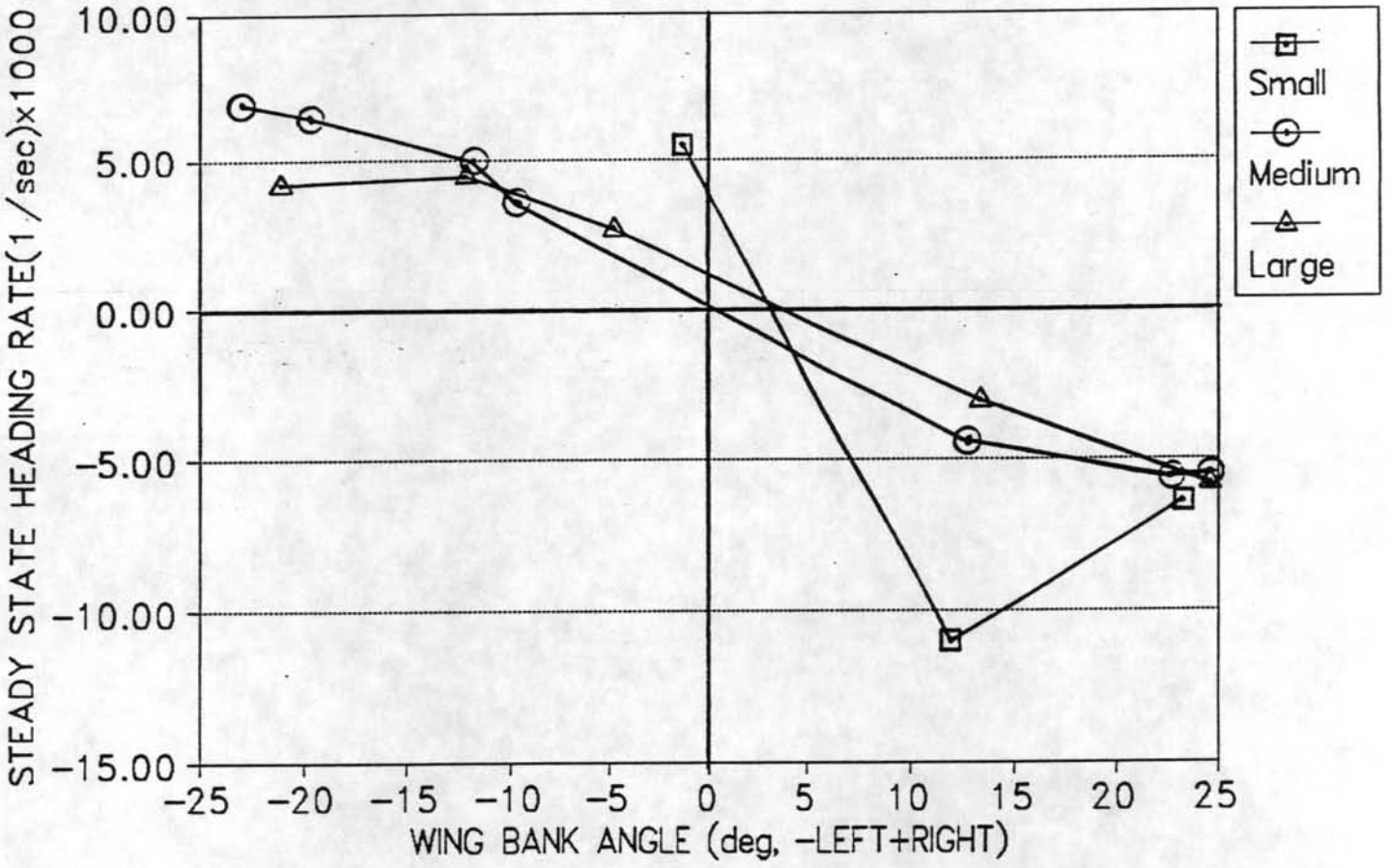

FIG. 12 (MEDIUM WINGS)
S.S. HEADING RATE VS BANK ANGLE

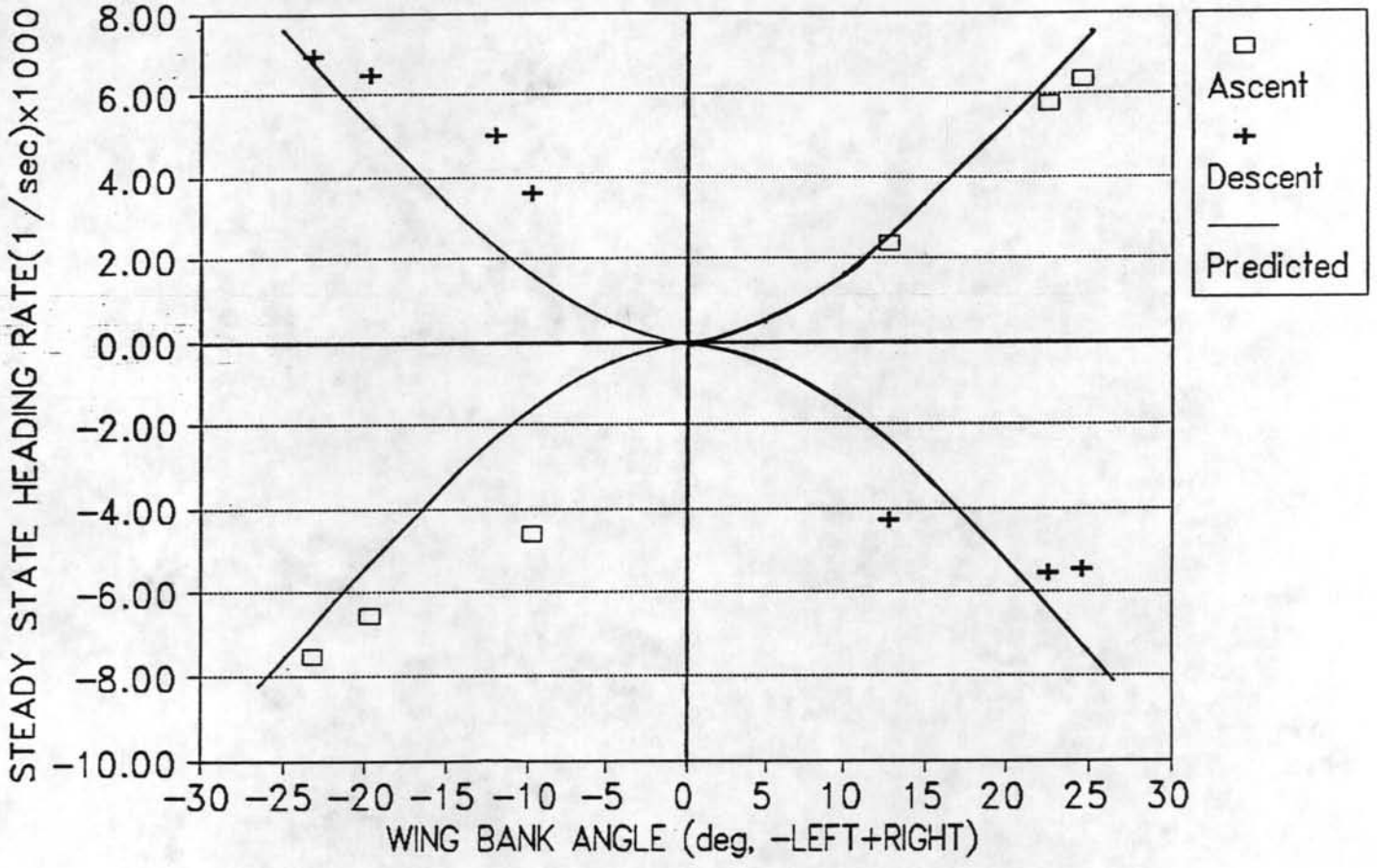

FIG. 13 (MEDIUM WINGS)
TURN RADIUS VS WING BANK ANGLE

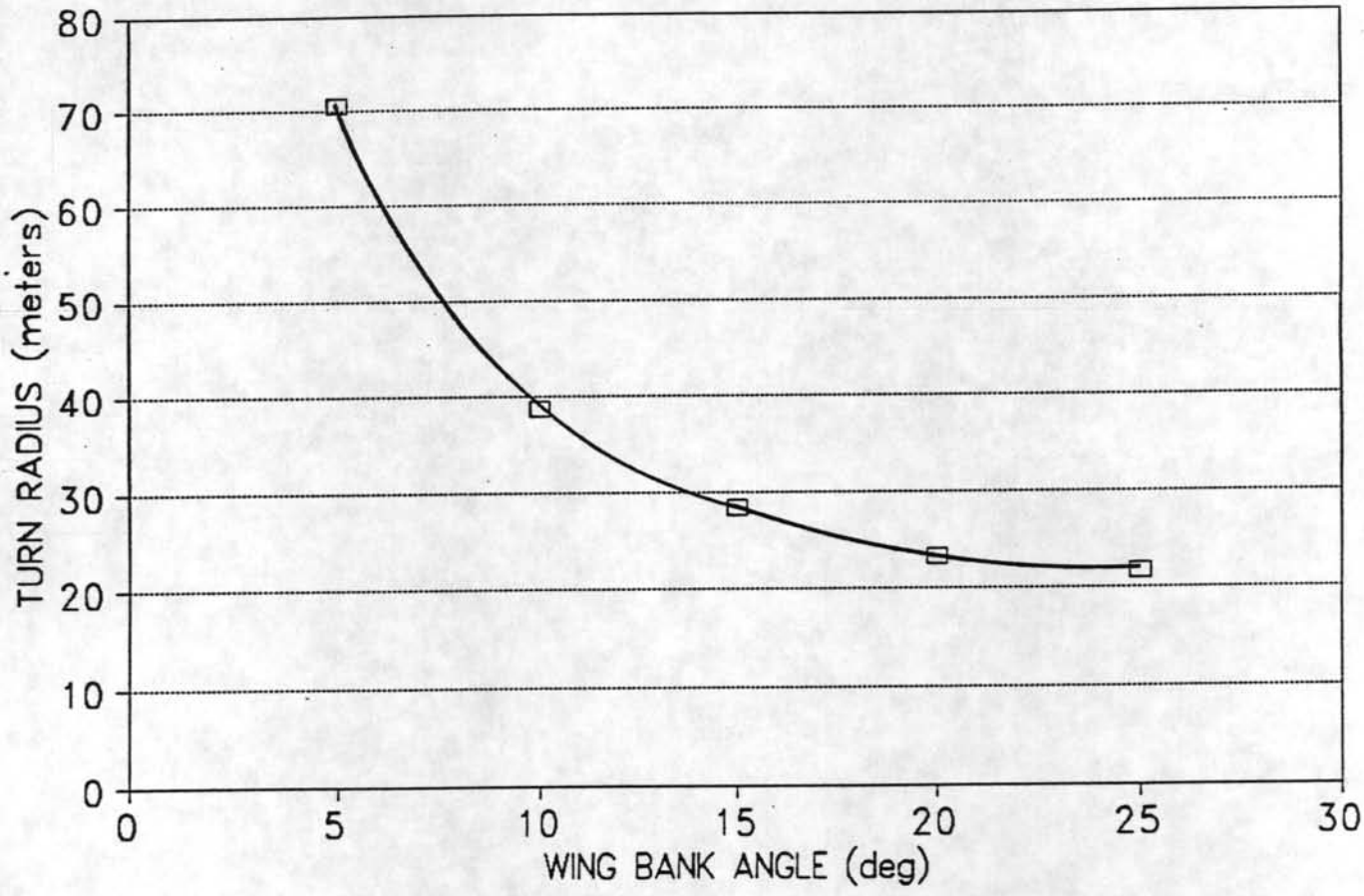

FIG. 14 (SMALL WINGS)
PITCH ANGLE VS TIME

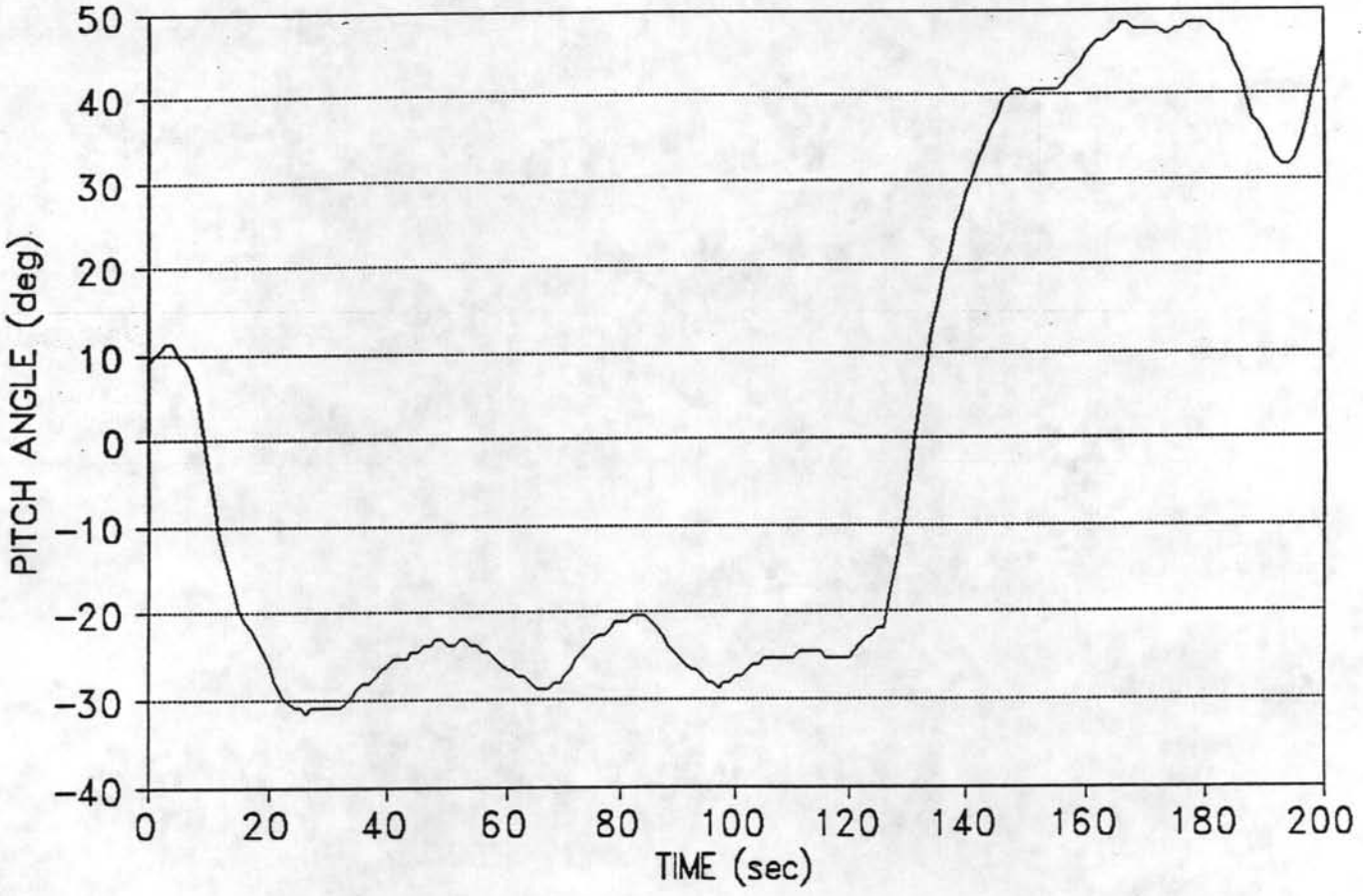

FIG. 15 (MEDIUM WINGS)
PITCH ANGLE VS TIME

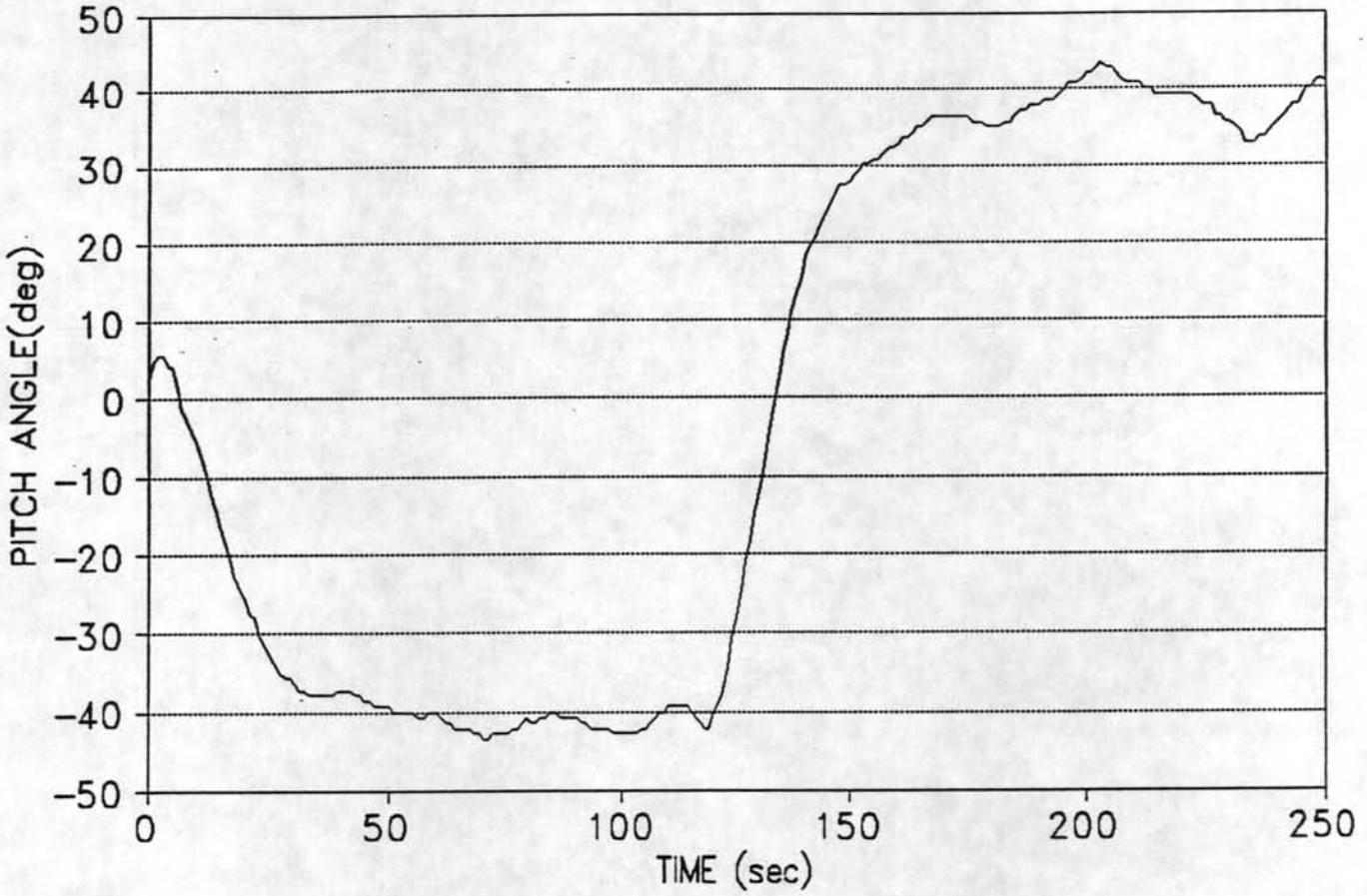

FIG. 16 (MEDIUM WINGS)
HEADING ANGLE VS TIME

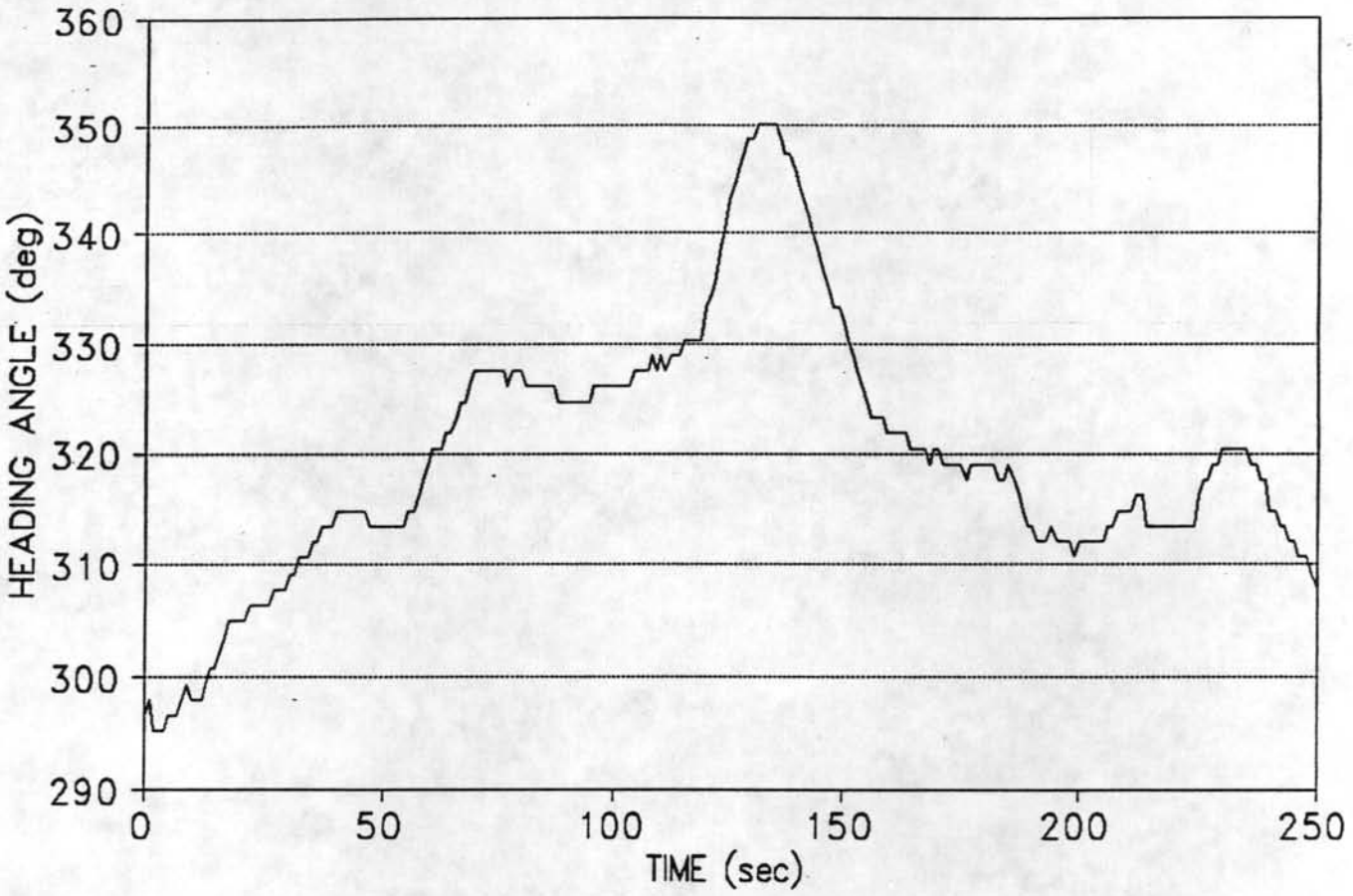

FIG. 17 (MEDIUM WINGS)
WING BANK ANGLE VS TIME

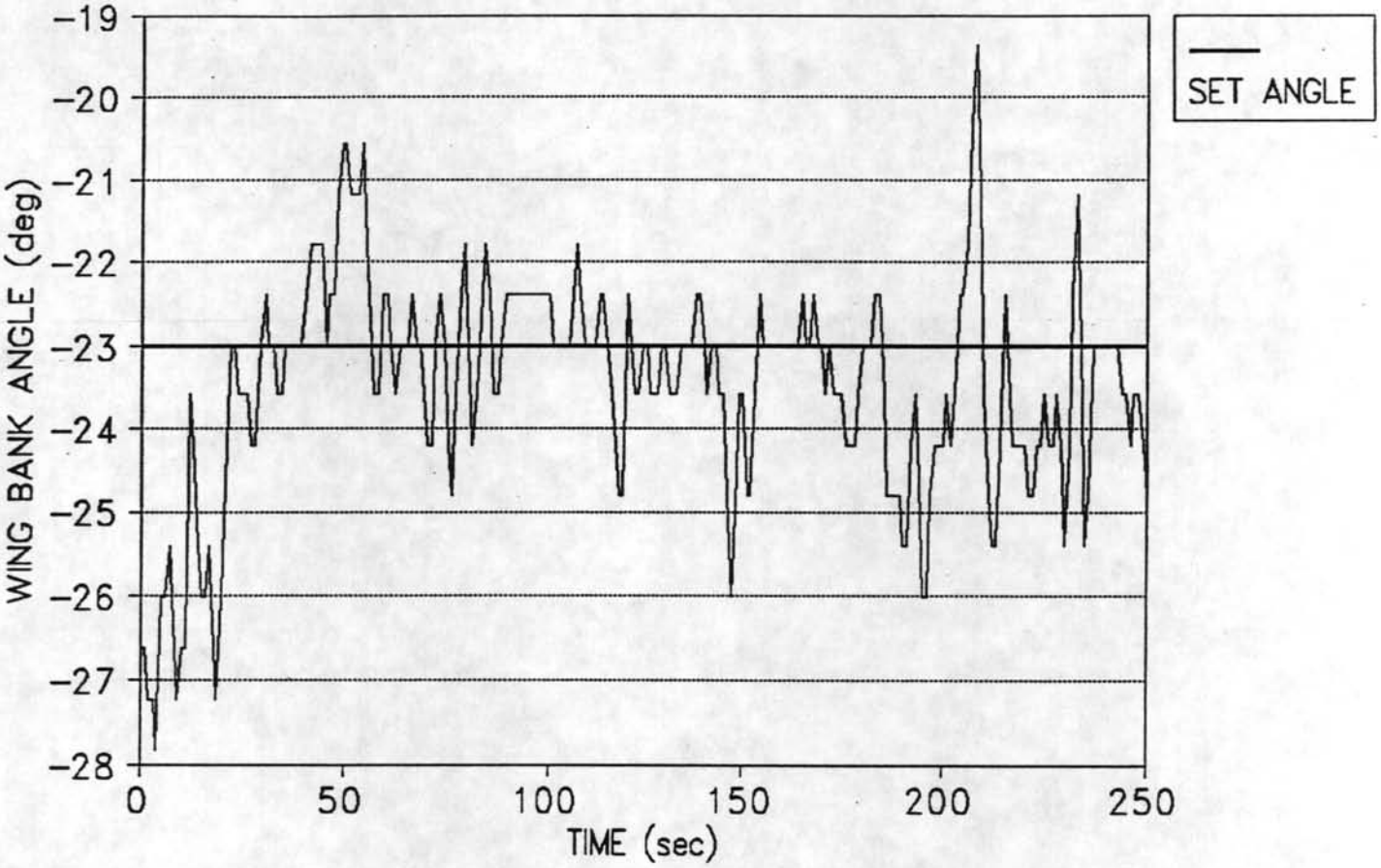

FIG.18 (LAKE TEST MODEL)
GLIDE SPEED VS PITCH ANGLE

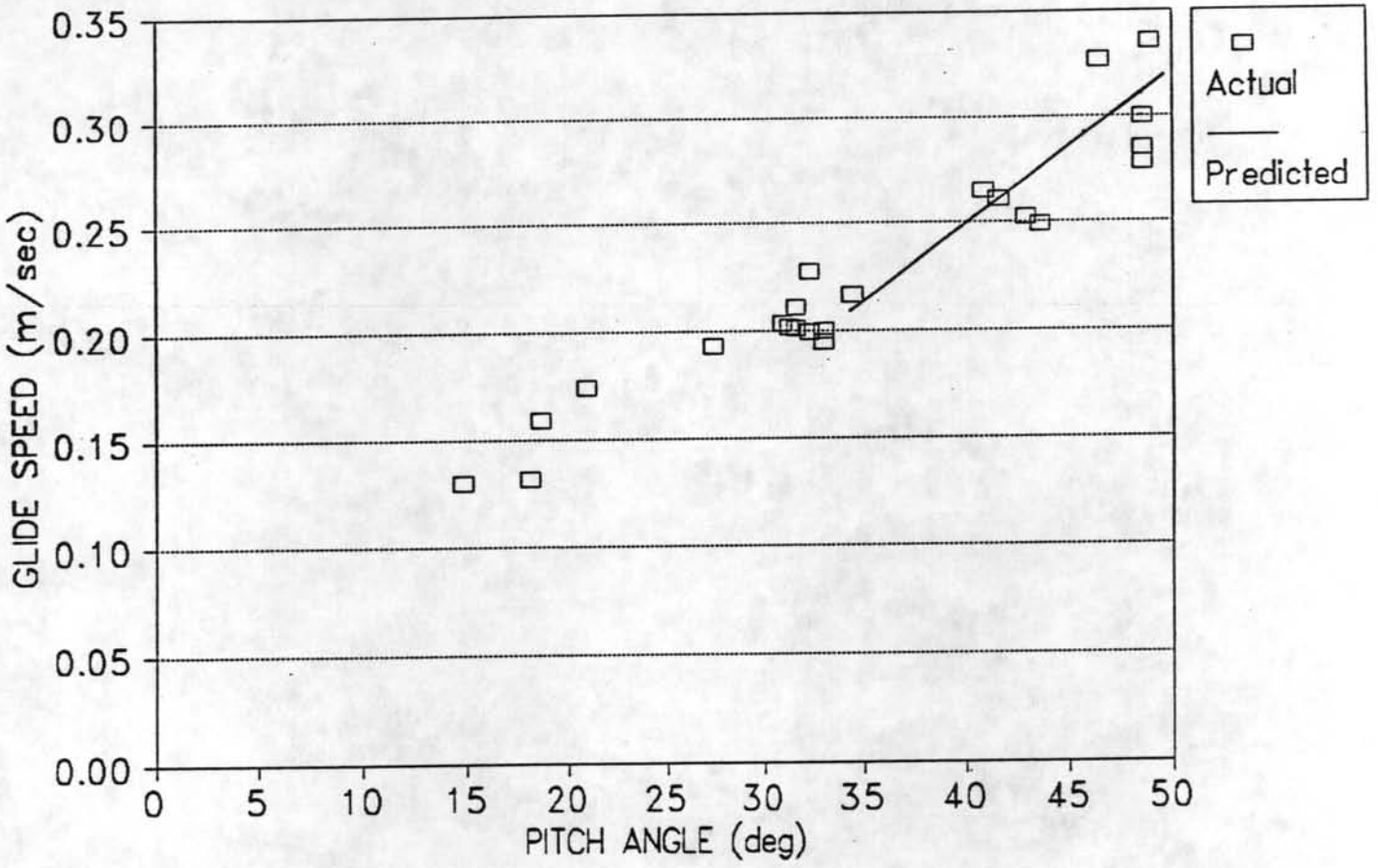

FIG.19 (LAKE TEST MODEL)
S.S.HEADING RATE VS BANK ANGLE

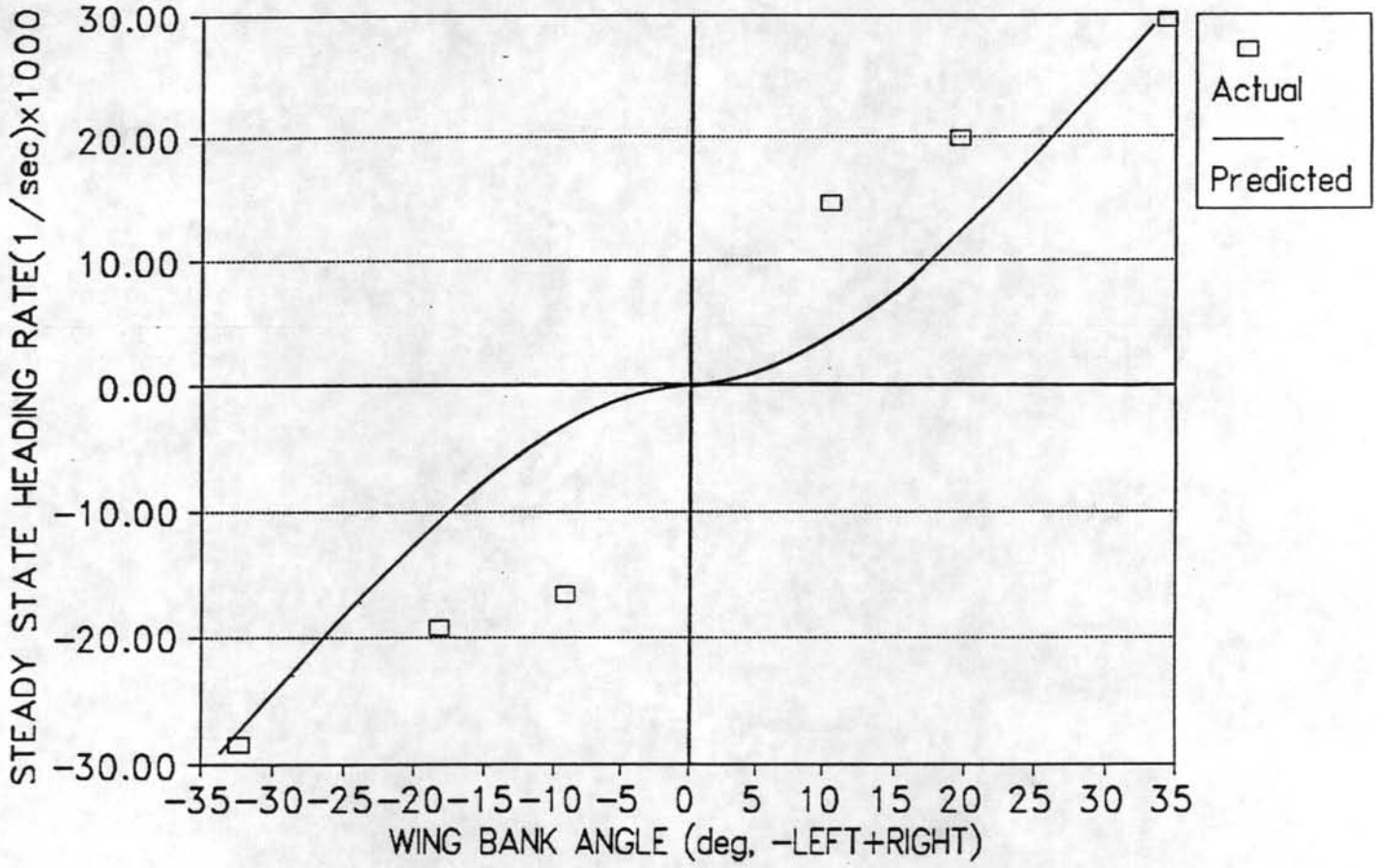

FIG.20 (LAKE TEST MODEL)
TURN RADIUS VS WING BANK ANGLE

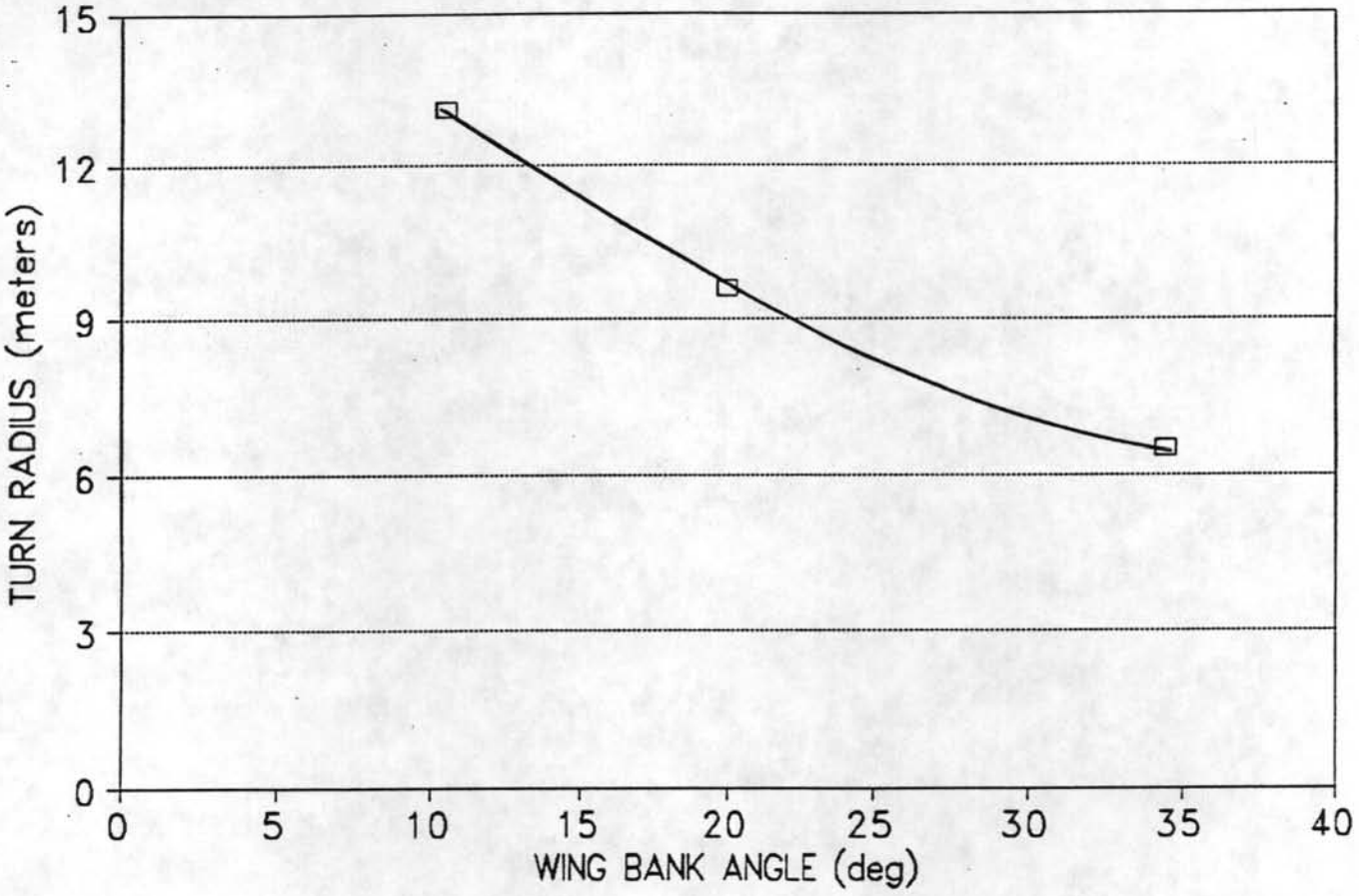

FIG.21 (LAKE TEST MODEL)
PITCH ANGLE VS TIME

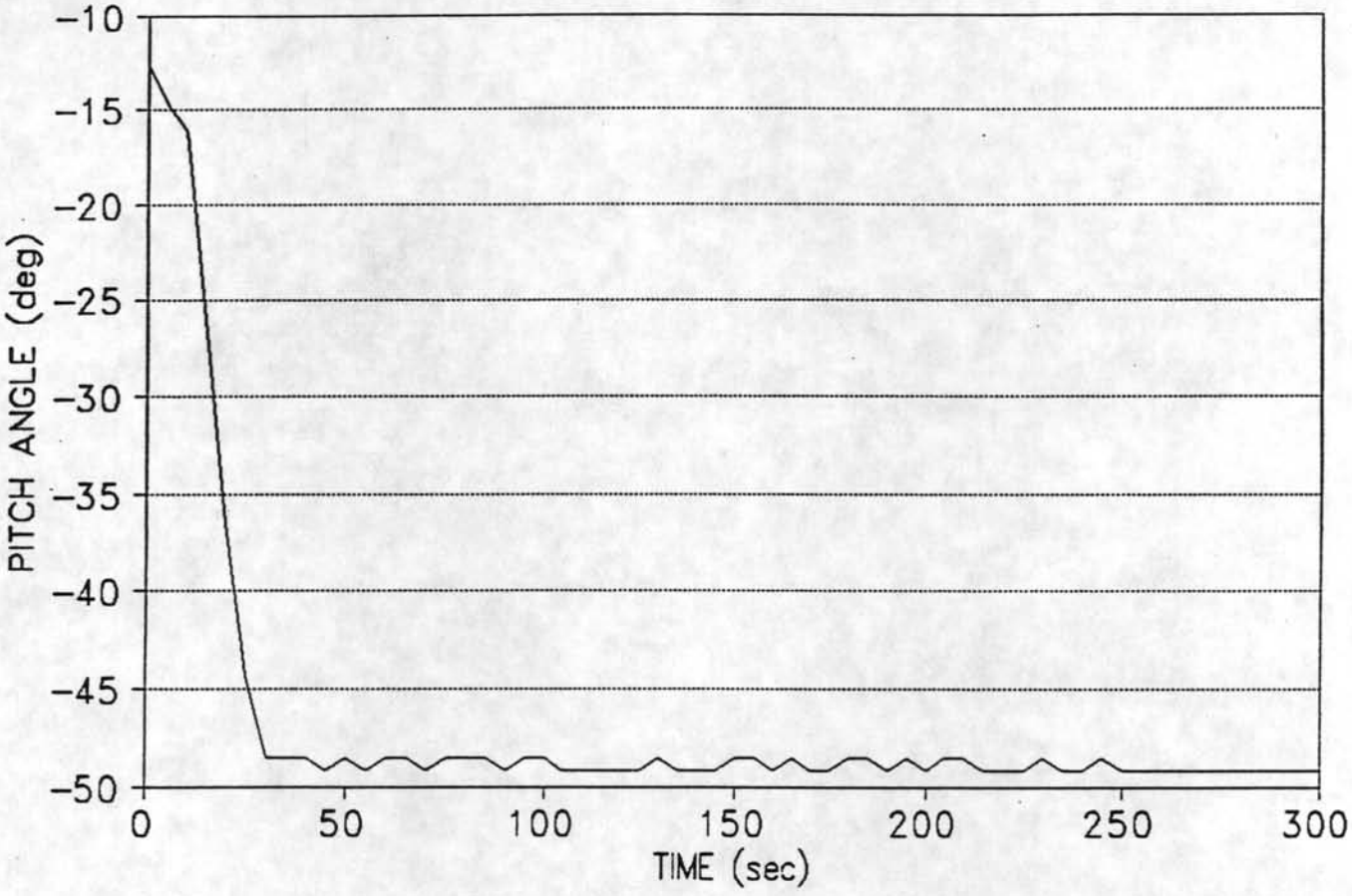

FIG.22 LAKE TEST MODEL
HEADING ANGLE VS TIME

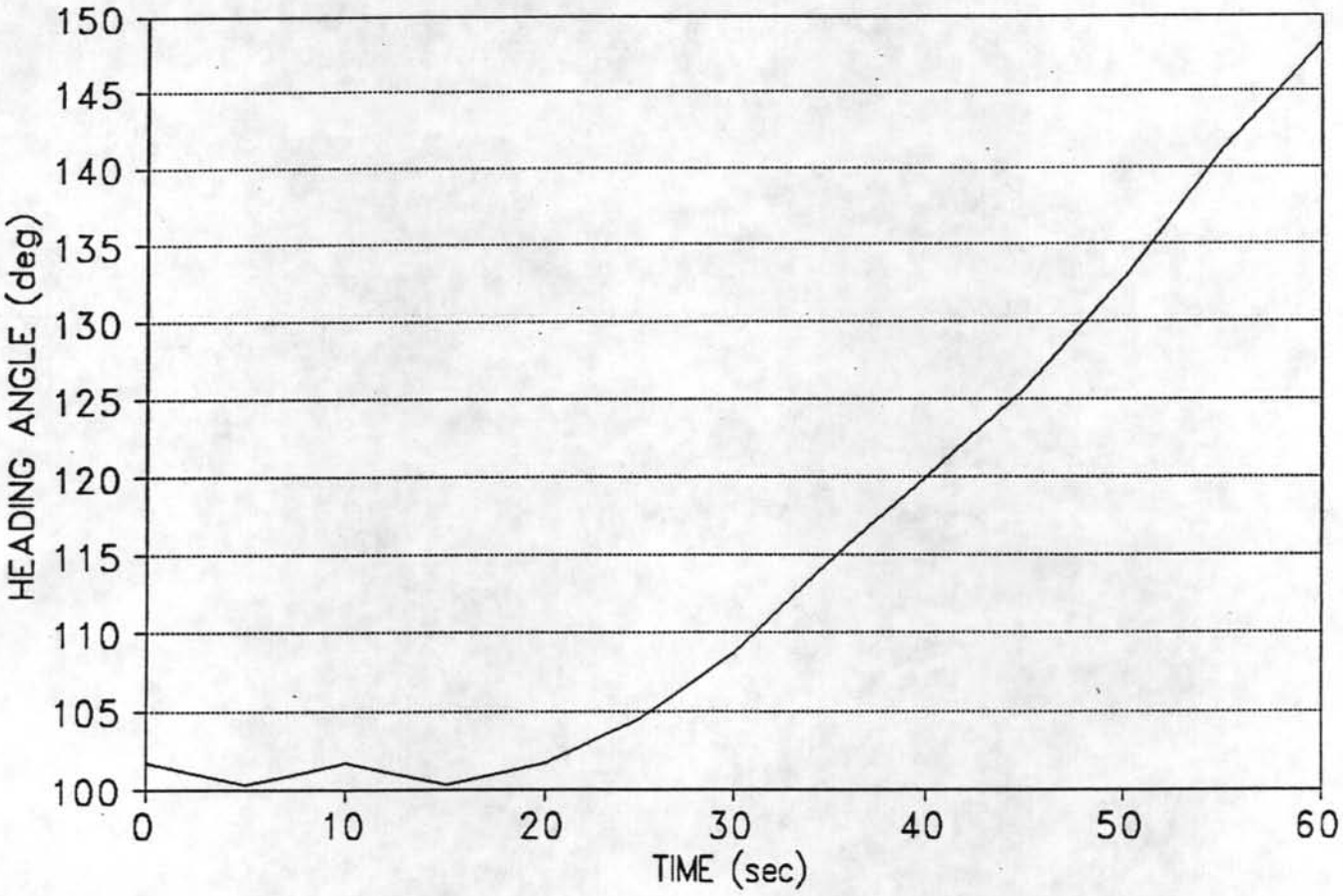

FIG.23 AUTOPILOT DIVE 7
GAIN[(1/sec)x1000]= 5.7

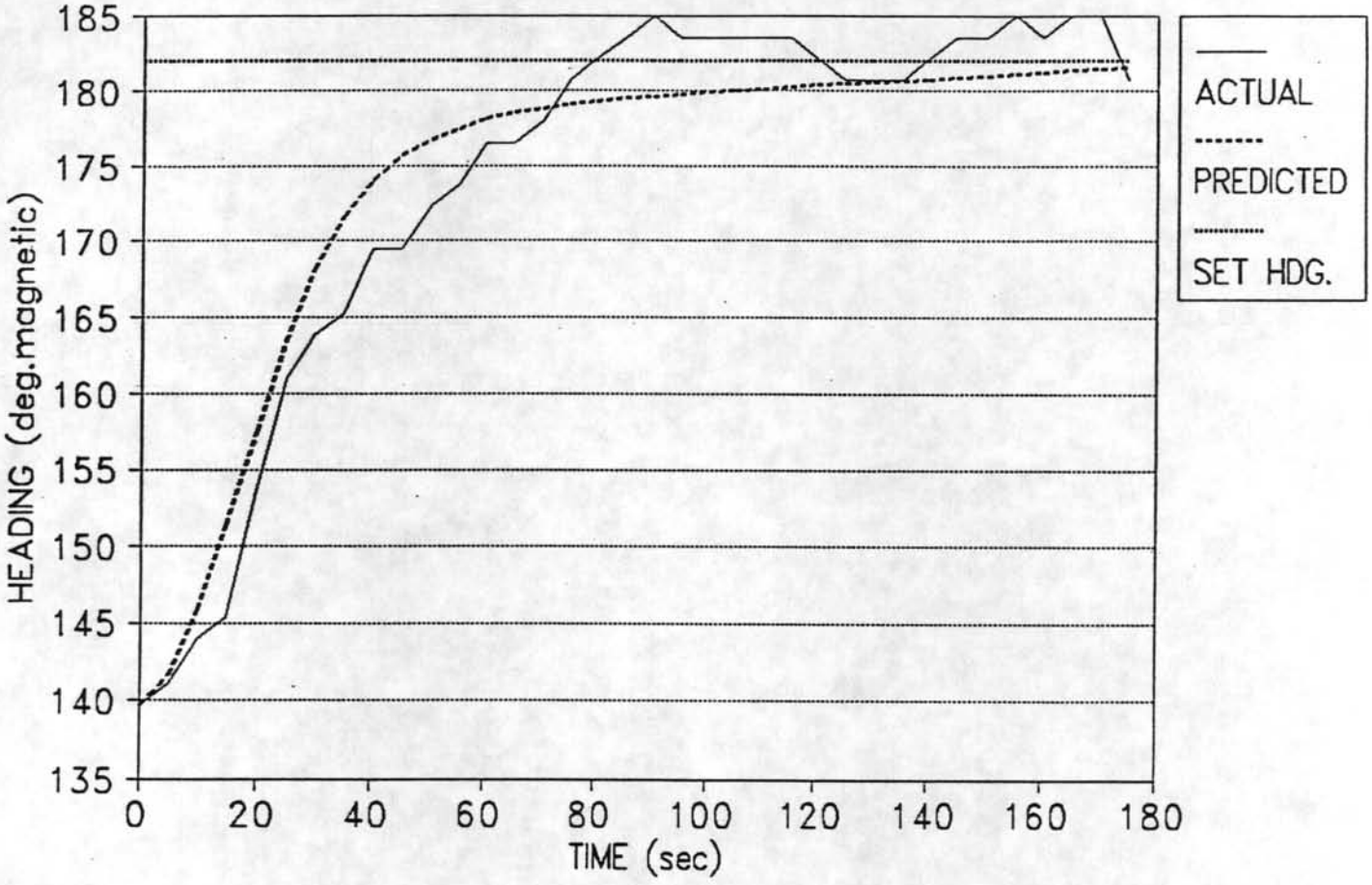

FIG.24 AUTOPILOT DIVE 7
WING ANGLE VS TIME

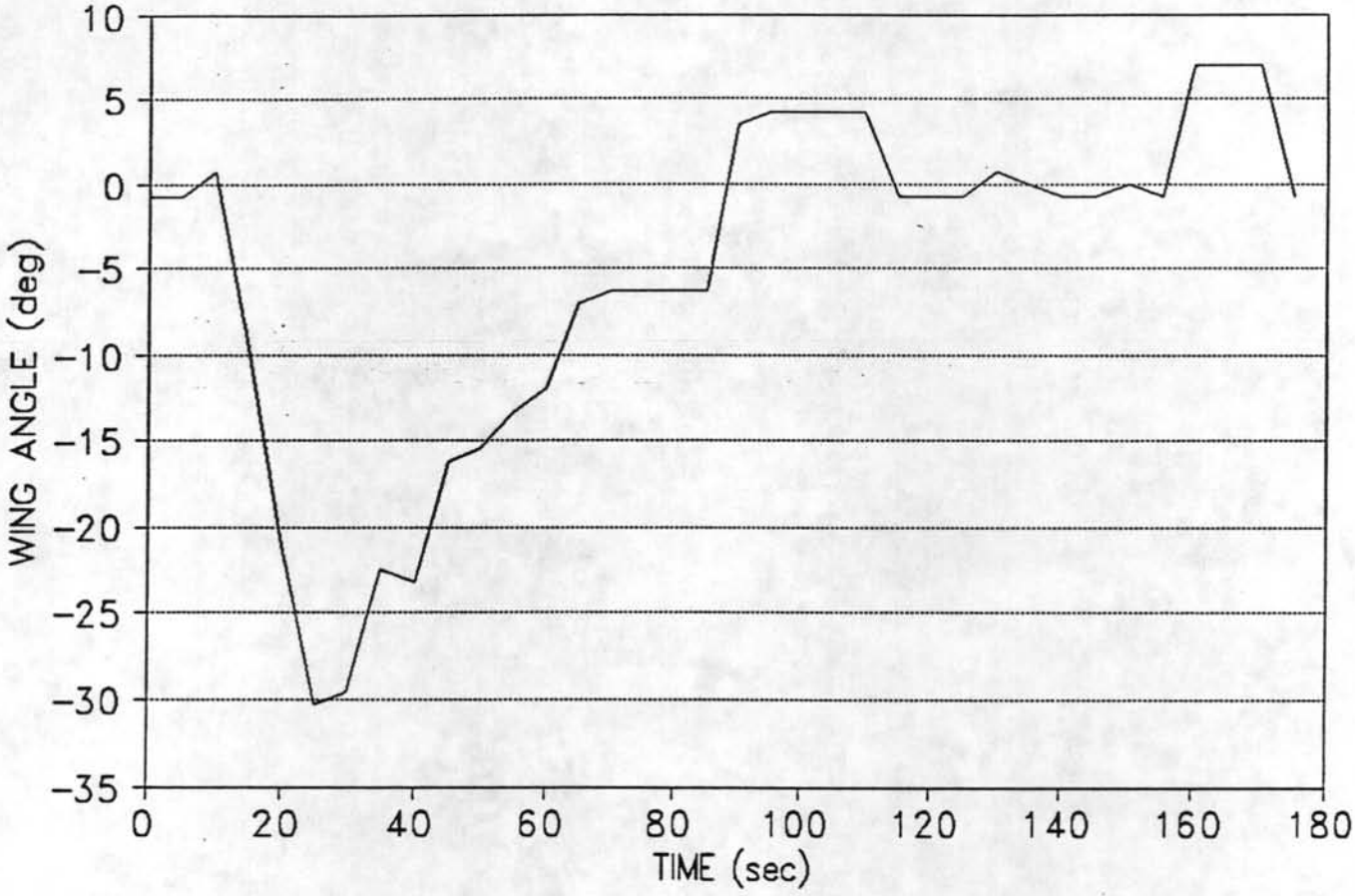

FIG.25 AUTOPILOT DIVE 9
GAIN[(1/sec)x1000]= 2.9

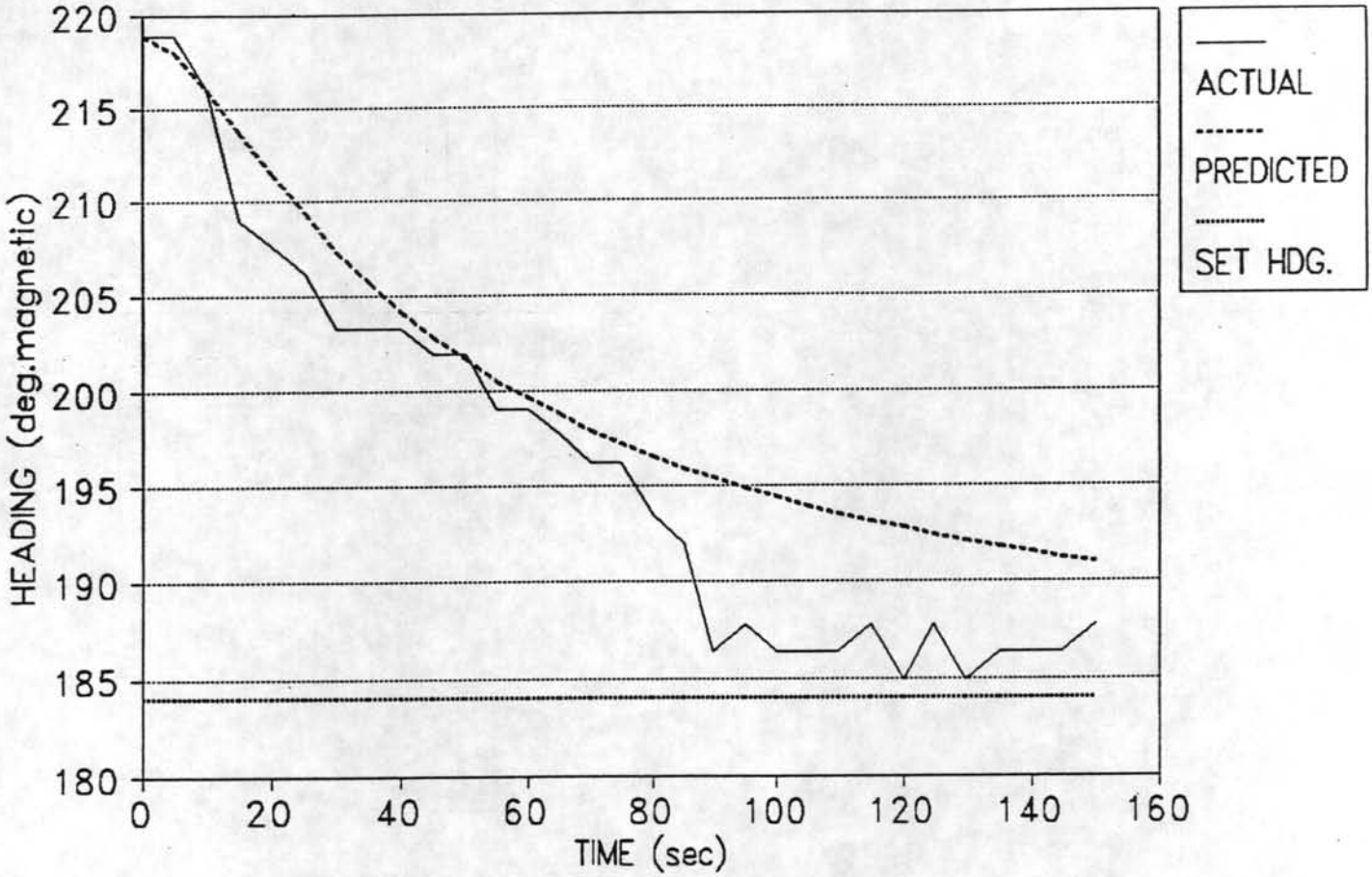

FIG.26 AUTOPILOT DIVE 10

GAIN[(1/sec)x1000]= 4.0